Identification of functionally-distinct macrophage subpopulations regulated by efferocytosis in *Drosophila*

Jonathon Alexis Coates[1], Amy Brittle[2], Emma Louise Armitage[2], Martin Peter Zeidler[1] & Iwan Robert Evans[2*]

[1] Department of Biomedical Science and the Bateson Centre, University of Sheffield, Sheffield, S10 2TN, UK

[2] Department of Infection, Immunity and Cardiovascular Disease and the Bateson Centre, University of Sheffield, Sheffield, S10 2TN, UK

[*] Correspondence: i.r.evans@sheffield.ac.uk

Short title: Macrophage subpopulations regulated by apoptosis in *Drosophila*

Abstract

Macrophages are a highly heterogeneous population of cells, with this diversity stemming in part from the existence of tissue resident populations and an ability to adopt a variety of activation states in response to stimuli. *Drosophila* blood cells (hemocytes) are dominated by a lineage of cells considered to be the functional equivalents of mammalian macrophages (plasmatocytes). Until very recently plasmatocytes were thought to be a homogeneous population. Here, we identify enhancer elements that label subpopulations of plasmatocytes, which vary in abundance across the lifecourse of the fly. We demonstrate that these plasmatocyte subpopulations behave in a functionally-distinct manner when compared to the overall population, including more potent migratory responses to injury and decreased clearance of apoptotic cells within the developing embryo. Additionally, these subpopulations display differential localisation and dynamics in pupae and adults, hinting at the presence of tissue-resident macrophages in the fly. Our enhancer analysis also allows us to identify novel candidate genes involved in plasmatocyte behaviour in vivo. Misexpression of one such enhancer-linked gene (*calnexin14D*) in all plasmatocytes improves wound responses, causing the overall population to behave more like the subpopulation marked by the *calnexin14D*-associated enhancer. Finally, we show that, we are able to modulate the number of cells within some subpopulations via exposure to increased levels of apoptotic cell death, thereby decreasing the number of plasmatocytes within more wound-responsive subpopulations. Taken together our data demonstrates the existence of macrophage heterogeneity in *Drosophila* and identifies mechanisms involved in the specification and function of these plasmatocyte subpopulations. Furthermore, this work identifies key molecular tools with which *Drosophila* can be used as a highly genetically-tractable, in vivo system to study the biology of macrophage heterogeneity.

Introduction

Macrophages are key innate immune cells responsible for clearing infections, debris and apoptotic cells, the promotion of wound healing and are necessary for normal development [1]. However, their aberrant behaviour can also cause or exacerbate numerous human disease states, including cancer, atherosclerosis and neurodegeneration [1]. Macrophages are a highly heterogeneous population of cells, which enables them to carry out their wide variety of roles, and this heterogeneity arises from diverse processes. These processes include the dissemination and maintenance of tissue resident populations [2] and the ability to adopt a spectrum of different activation states (termed macrophage polarisation), which can range from pro-inflammatory (historically termed as M1-like) to anti-inflammatory, pro-healing (M2-like) macrophage activation states [3,4].

Macrophage heterogeneity appears to be conserved across jawed vertebrate lineages. Evidence suggests the existence of pro-inflammatory macrophage populations [5] and myeloid-derived microglia in zebrafish [6,7], with polarisation also a well-defined phenomenon in other fish species [8]. Vertebrate macrophages interact with and can become polarised in response to signals produced by Th1 and Th2 cells, leading to acquisition of M1-like and M2-like activation states, respectively. To date this form of heterogeneity has been considered to be restricted to organisms containing both an adaptive and an innate immune system. B and T cell-based adaptive immunity is thought to have evolved in teleost fish [9] and the diversity of macrophage populations in organisms possessing only an innate immune system appears more restricted. However, even comparing mammals as closely related as mice and humans, macrophage markers can be highly divergent [10], therefore other approaches and markers might be required to identify equivalent macrophage diversity in lower organisms.

Macrophage heterogeneity has been extensively studied in mammalian systems and, although this has provided a good understanding of how macrophages determine their polarisation state, this has also identified considerable complexity with many activation states possible [11]. Additional complexity arises with both M1-like and M2-like macrophages found at the same sites of pathology, for example within atherosclerotic plaques [12]. Furthermore, the cytokine profiles that can be induced in vitro depend on the exact activation methods used experimentally and these do not necessarily reflect polarisation states in vivo [13], while other macrophage subpopulations may be missed by in vitro approaches. Given these intricacies, it is clear that we still need to better understand the fundamental components and pathways responsible for the specification of different macrophage subtypes, particularly in vivo. Recently the "macrophage-first" hypothesis has been proposed, re-emphasising the idea that acute signals polarise macrophages ahead of the involvement of T cells [8]. Consequently, organisms without a fully-developed adaptive immune system represent intriguing models in which to examine this idea and better understand macrophage heterogeneity in vivo.

Drosophila melanogaster has been extensively used to study innate immunity [14], but lacks an adaptive immune system. Fruit flies possess three types of blood cell (also referred to as hemocytes): plasmatocytes, crystal cells and lamellocytes. Of these, plasmatocytes are functionally equivalent to vertebrate macrophages [15,16], with the capacity to phagocytose apoptotic cells and pathogens, secrete extracellular matrix, disperse during development and migrate to sites of injury [17]. Although *Drosophila* blood lineages are considerably less complex than their vertebrate equivalents, they are specified via transcription factors related to those used during vertebrate myelopoiesis, including GATA and Runx-related proteins [15]. Furthermore, plasmatocytes utilise evolutionarily-conserved genes in common with vertebrate innate immune cells to migrate (e.g. SCAR/WAVE, integrins and Rho GTPases [18–22]) and phagocytose (e.g. the CED-1 family member Draper [23] and CD36-related receptor Croquemort [24]). Given these striking levels of functional

and molecular conservation, *Drosophila* has been extensively used for research into macrophage behaviour in vivo with its genetic tractability and in vivo imaging capabilities facilitating elucidation of different macrophage behaviours conserved through evolution [16,17]. However, despite these evolutionarily-conserved commonalities, the plasmatocyte lineage has, until very recently, been considered a homogeneous cell population. Hints that *Drosophila* plasmatocytes may exhibit heterogeneity exist in the literature with variation in marker expression observed in larval hemocytes [25] and non-uniform expression of TGF-β homologues upon injury or infection in adults [26]. Recent single-cell RNA-sequencing (scRNA-seq) experiments performed on larval hemocytes demonstrated the presence of multiple clusters of cells, which were interpreted as representing either different stages of differentiation or functional groupings [27,28]. However, the in vivo identification of subtypes and insights into the roles and specification mechanisms of potential macrophage subtypes in *Drosophila* has not yet been described.

Here, we describe the first identification and characterisation of molecularly and functionally-distinct plasmatocyte subpopulations within *Drosophila melanogaster*. Drawing on a collection of reporter lines [29], we have identified regulatory elements that define novel plasmatocyte subpopulations in vivo. We show that these molecularly-distinct subpopulations exhibit functional differences compared to the overall plasmatocyte population and that the proportions of cells within these subpopulations can be modulated by external stimuli such as increased levels of apoptosis. Furthermore, we show that misexpression of a gene associated with a subpopulation-specific enhancer element is able to modulate plasmatocyte behaviour in vivo, thereby identifying novel effector genes of plasmatocyte subpopulation function. Together our findings reveal that macrophage heterogeneity is a fundamental and evolutionarily-conserved characteristic of innate immunity that pre-dates the development of the adaptive immune system. This significantly extends the utility of an already powerful genetic model system and provides further avenues to understand regulation of innate immunity and macrophage heterogeneity.

Results

Drosophila embryonic plasmatocytes do not behave as a uniform population of cells

The macrophage lineage of hemocytes (plasmatocytes) has historically been considered a homogeneous population of cells. However, careful analysis of plasmatocyte behaviour in vivo suggested to us that this lineage might not be functionally uniform. For instance, imaging the inflammatory responses of plasmatocytes to epithelial wounds, we find that some cells close to injury sites rapidly respond by migrating to the wound, while other neighbouring cells fail to respond, (Figure 1a; Supplementary Movie 1). We also find that plasmatocytes exhibit variation in their expression of well-characterised plasmatocyte markers (*crq-GAL4* [19,24]*;* Figure 1b-b') and display a broad diversity in their migration speeds within the embryo (random migration at stage 15, Figure 1c-d). These professional phagocytes also display differences in their capacities to phagocytose apoptotic cells with some cells engulfing many apoptotic particles, whereas others engulf very few, if any (Figure 1e). Furthermore, phagocytosis of microorganisms by larval hemocytes also varies significantly from cell-to-cell in vitro (Figure 1f). These differences within the plasmatocyte lineage led us to hypothesise that this cell population is more heterogeneous than previously appreciated.

Figure 1. Heterogeneity of *Drosophila* embryonic plasmatocyte responses

(a) GFP (green) and nuclear red stinger (magenta) labelled plasmatocytes on the ventral side of a stage 15 embryo at 0-minutes (a) and 60-minutes post-wounding (a'); plasmatocyte tracks at each timepoint are overlaid and shown in full in a''. Examples of plasmatocytes that fail to respond to the wound indicated via asterisks; "w" shows centre of the wound; square bracket in (a) shows neighbouring plasmatocytes, one of which responds to wounding, the other fails to respond (see Supplementary Movie 1). (b) imaging of plasmatocytes labelled using *crq-GAL4* to drive expression of

144 GFP reveals a wide range in levels of *crq* promoter activity within plasmatocytes at stage 15; (b')
145 shows zoom of cells marked by an asterisk in (b). (c) overlay of plasmatocyte tracks of cells shown in
146 (b) showing significant variation in their random migration speeds. (d) scatterplot of plasmatocyte
147 random migration (rm) speeds (taken from 23 embryos); line and error bars show mean and
148 standard deviation, respectively. (e) imaging the ventral middle at stage 15 shows a wide range in
149 the amount of apoptotic cell clearance (green in merge, labelled via the caspase-sensitive reporter
150 GC3ai) undertaken by plasmatocytes (magenta in merge, labelled via *srp-3x-mCherry* reporter); (e')
151 and (e'') show mCherry and GC3ai channels alone; (e''') shows zoomed examples of cells devoid/full
152 of engulfed GC3ai particles, which are indicated by asterisks in (e). (f) larval hemocytes (green in
153 merge, labelled via *hml(Δ)-GAL4* driven expression of GFP) exhibit a range in their capacities to
154 engulf calcofluor-labelled yeast (blue in merge) in vitro; (f') and (f'') show GFP and yeast channels
155 alone, respectively; white lines indicate cell edges in (f''); asterisks in (f'') indicate cells that have
156 failed to phagocytose yeast; white arrows in (f'') indicate cells that have phagocytosed multiple yeast
157 particles; magenta arrow in (f'') indicates zoomed region shown in (f'''). Scale bars represent 20μm
158 (a-a'', b, c, e-e''), 10μm (e''', f-f''), or 5μm (b', f'''). See Supplementary Table 1 for full list of
159 genotypes.
160

161 **Discrete subpopulations of plasmatocytes are present in the developing *Drosophila***
162 **embryo**

163 Given the diversity in plasmatocyte behaviour (Figure 1), we hypothesised that macrophage
164 heterogeneity represents an evolutionarily-conserved feature of innate immunity, which therefore
165 originally evolved in the absence of an adaptive immune system. To address this and look for
166 molecular differences between plasmatocytes, we examined transgenic enhancer reporter lines (*VT-*
167 *GAL4* lines) produced as part of a recent large-scale tilling array screen [29] that had been annotated
168 as labelling hemocytes (http://enhancers.starklab.org/). Based on examination of the published *VT-*

169 *GAL4* expression patterns, we identified *VT-GAL4* lines that appeared to label reduced numbers of
170 plasmatocytes in the embryo, reasoning that plasmatocyte subpopulations could be molecularly
171 identified on the basis of differences in reporter expression. While a number of the enhancers
172 appeared to label all plasmatocytes (e.g. *VT41692-GAL4*), we identified several that labelled discrete
173 numbers of plasmatocytes (Figure 2a). We next confirmed that the cells labelled by these *VT-GAL4*
174 lines were plasmatocytes by using these constructs to drive expression of *UAS-tdTomato* in the
175 background of a *GAL4*-independent, pan-hemocyte marker (*srp-GMA* (GFP-tagged actin-binding
176 domain of moesin); Figure 2b-d; [30]). As initially predicted based on their morphology and position
177 during embryogenesis, each of the *VT-GAL4* lines marking potential subpopulations did indeed
178 express in the hemocyte lineage Figure 2e). These subpopulation cells were identified as
179 plasmatocytes based upon their morphology, the absence of lamellocytes in embryos and the non-
180 migratory nature of crystal cells (Figure 2e; [16]) and could be observed to follow both the dorsal
181 and ventral migration routes [17] used by these cells during their developmental dispersal (Figure
182 2e). In order to quantify the proportion of cells labelled by each *VT-GAL4* line, we counted the
183 number of cells labelled on the ventral midline of the developing stage 15 embryo, using *VT-GAL4*
184 lines to drive GFP expression. This verified reproducible and consistent labelling of discrete subsets
185 of plasmatocytes (Figure 2f-h), suggesting that these cells represent stable subpopulations within
186 this macrophage lineage.
187

188 **Figure 2. Enhancers labelling plasmatocyte subpopulations in *Drosophila***
189 (a) lateral views of stage 13/14 embryos with in situ hybridisation performed for *GAL4* for indicated
190 *VT-GAL4* lines (anterior is left). Taken with permission from http://enhancers.starklab.org/ (n.b.
191 Stark Lab retain copyright of these images); *VT41692-GAL4* represents an example in which the
192 majority of plasmatocytes are labelled. (b) schematic diagram showing screening approach to
193 identify subpopulations of plasmatocytes: *VT-GAL4* positive plasmatocytes will express both GMA
194 (green) and tdTomato (magenta) – white cells in the schematic. (c-d) images showing the ventral

195 midline at stage 14 of negative control (no driver; *w;UAS-tdTom/+;srp-GMA*) and positive control
196 (w;*srp-GAL4/UAS-tdTom;srp-GMA*) embryos. (e) images showing embryos containing *VT-GAL4*
197 labelled cells (via *UAS-tdTomato*, shown in magenta) at stage 13 (first row, ventral views), stage 14
198 (second row, dorsal views) and stage 15 (third row, ventral views). The entire hemocyte population
199 is labelled via *srp-GMA* (green); arrows indicate examples of *VT-GAL4* positive plasmatocytes;
200 asterisks indicate *VT-GAL4* positive cells that are not labelled by *srp-GMA*. N.b. *VT62766-GAL4* image
201 contrast enhanced to different parameters compared to other images owing to the very bright
202 labelling of amnioserosal cells (cells on dorsal side of embryo destined to be removed during dorsal
203 closure; labelled with an asterisk) in the stage 14 image. (f) labelling of smaller numbers of
204 plasmatocytes on the ventral midline at stage 15 using *VT-GAL4* lines indicated and *UAS-GFP* (green);
205 boxed regions show zooms of *VT-GAL4* positive plasmatocytes (f'). (g) ventral view of positive
206 control embryo (*w;srp-GAL4/+;UAS-GFP*) and example plasmatocyte (g') at stage 15. (h) scatterplot
207 showing quantification of numbers of *VT-GAL4,UAS-GFP* labelled plasmatocytes on the ventral
208 midline at stage 15; lines and error bars represent mean and standard deviation, respectively. P-
209 values calculated via one-way ANOVA with a Dunnett's multiple comparison post-test (all compared
210 to *srp-GAL4* control; n=9 embryos per genotype. All scale bars represent 10μm. See Supplementary
211 Table 1 for full list of genotypes.
212

213 **Subpopulations of *Drosophila* plasmatocytes vary across development: subpopulation**
214 **dynamics in larvae and white pre-pupae**

215 Having identified subpopulations of plasmatocytes in the embryo, we then tested other stages of the
216 life cycle to see how expression might be maintained or modulated throughout development. In
217 order to exclude potential expression in non-hemocyte cells (e.g. non-plasmatocyte cells apparent in
218 Figure 2e), we labelled subpopulation cells specifically using a split GAL4 approach [31], via which
219 only cells expressing both *serpent* (a well-characterised hemocyte marker; [32]) and the named VT

enhancer would be labelled via transcriptional activation of *UAS* transgenes (Supplementary Figure 1).

Imaging of L3 larvae containing split GAL4 constructs (*srp-AD;VT-DBD* – henceforth abbreviated to *VTn*) driving *UAS-stinger* revealed that very few subpopulation cells were present at this stage (Figure 3a-f). From larval development onwards, we cannot use cell morphology to discriminate between plasmatocytes and other hemocyte lineages (crystal cells and lamellocytes) and therefore refer to subpopulation cells as hemocytes for these subsequent stages. Using this approach, *VT32897* and *VT17559* labelled the most cells (Figure 3c-d), with only the occasional cell present in *VT57089* larvae (Figure 3e) and cells essentially absent from *VT62766* larvae (Figure 3f). Labelled cells were also present in the head region, along the dorsal vessel (the fly heart) and between the salivary glands (which exhibit non-specific labelling) in *VT32897* larvae. The *VT32897* head region cells are potentially specifically localised hemocytes, whereas cells at the remaining two sites are likely to correspond to *serpent*-positive nephrocytes and garland cells [33,34], respectively (Figure 3d). *VT57089* shows additional staining in the head region (potentially the Bolwig organ; Figure 3e) and, as per the dorsal vessel-associated cells in *VT32897* (Figure 3d), this can be observed in positive controls (data not shown). These patterns closely resemble patterns observed using the initial *VT-GAL4* reporters, albeit with more restricted labelling due to our split GAL4 approach (data not shown).

Figure 3. Plasmatocyte subpopulations in larvae and white pre-pupae

(a-f) dorsal and ventral views of L3 larvae lacking *GAL4* (a, negative control), with hemocytes labelled (b, positive control with *UAS-stinger* driven by *srp-AD;srp-DBD*), or with cells labelled through expression of *UAS-stinger* via *srp-AD* and the *VT-DBD* transgenes indicated (c-f); non-specific expression of Stinger in salivary glands and gut autofluorescence is visible in (a') and (c'-f') and is indicated by an arrow and asterisk, respectively, in (a'). Arrows/asterisks indicate regions containing

circulating hemocytes (c), potential hemocyte population in the head region (d), possible proventricular region/garland cells (d'), cells in the Bolwig organ (arrow in e), and rare circulating hemocytes labelled via *srp-AD;VT57089-DBD* (asterisk in e) that are shown as zooms in inset images. (f") shows region indicated by bar in (f) at a reduced brightness to reveal detail of cells along the dorsal vessel. (g-h) dorsal and ventral views of negative control (g, *UAS-stinger* but no driver) and positive control (h, *UAS-stinger* driven by *srp-AD;srp-DBD*) white pre-pupae (WPP). (i-l) VT enhancer-labelled cells are almost completely absent from WPP (*srp-AD;VT-DBD* transgenes used to drive *UAS-stinger* expression). All scale bars represent 500µm; images contrast enhanced to 0.3% saturation. See Supplementary Table 1 for full list of genotypes.

Imaging of white pre-pupae (WPP), the stage that marks the beginning of pupal development and metamorphosis, showed very similar patterns across the split GAL4 VT enhancer lines (Figure 3g-l), but with a further reduction in the numbers of cells labelled. It was possible to observe the occasional cell moving in circulation within WPP, strongly suggesting these cells are hemocytes (Supplementary Movies 2 and 3). Live imaging of *VT32897* WPP also confirmed association of cells with the pumping dorsal vessel (Supplementary Movie 4). Significantly, this data indicates that the presence of subpopulations within embryos is not simply a consequence of slow accumulation of fluorescent proteins by weak drivers, since these enhancer-based reporters do not label an ever-increasing number of cells as development proceeds. Overall, the numbers of hemocytes within subpopulations decreases over larval and early pupal stages demonstrating that plasmatocyte subpopulations are developmentally regulated. Such changes could reflect specific and changing requirements for specialised plasmatocyte subpopulations across the life cycle, for example an association with processes required for organogenesis [35–37]. This specific localisation of subpopulation cells also indicates the potential for tissue-resident macrophages in *Drosophila*.

Subpopulation cells return in large numbers during pupal development

Since subpopulation cells appear associated with stages of development when organogenesis and tissue remodelling occurs, we hypothesised that hemocyte subpopulations would return during metamorphosis. Imaging pupae at various times after puparium formation (APF) revealed that subpopulation cells re-emerged in large numbers during this stage, but with distinct dynamics (Figure 4a-f): *VT17559* cells have already returned in very substantial numbers by 18h APF (Figure 4c), whereas *VT32897* reporter expression reappeared between 24 and 48h APF (Figure 4d). *VT57089* and *VT62766*-labelled cells increased in numbers more gradually over the course of pupal development (Figure 4e-f).

Figure 4. Plasmatocyte subpopulations return with distinct dynamics during pupal development

(a-b) dorsal images of negative control (lacking *GAL4* drivers, a) and positive control pupae (labelled via *srp-AD;srp-DBD*, b) at 18h after puparium formation (APF). (c-f) dorsal images showing localisation of cells labelled using *srp-AD* and *VT-DBD* (VT enhancers used to drive *DBD* expression indicated above panels) to drive expression of *UAS-stinger* during pupal development from 18h AFP to 72h APF (c-f). All image panels contrast enhanced to 0.3% saturation to reveal localisation of labelled cells due to differing intensities of reporter line expression. Scale bars represent 500µm. See Supplementary Table 1 for full list of genotypes.

Subpopulations display distinct dynamics and localisation in adults

Immediately after adults hatch, large numbers of split GAL4-labelled cells can be observed across all lines and are present in selective regions that overlap with the overall adult hemocyte population (Figure 5a-e). The overall hemocyte population remains detectible as adults age (0-6 weeks; Figure 5a), however not all subpopulations exhibit an identical localisation or dynamics during this time

(Figure 5b-e). *VT57089* and *VT62766* cells largely disappear by 1 week (Figure 5d-e) and the majority of *VT17559*-labelled cells are absent by 2 weeks (Figure 5b). By contrast, *VT32897* cells persist for at least 6 weeks of adult life and are particularly prominent in the thorax at 4 weeks (Figure 5c). Other differences in localisation are also apparent with cells particularly obvious in the legs for the *VT17559* line (Figure 5b, day 1-2 weeks), whereas *VT57089* and *VT62766*-labelled cells are more closely associated with the thorax and dorsal abdomen (Figure 5d-e, day 1). Labelled cells are also present in the proboscis for several lines (Figure 5c-e). The distinct dynamics of subpopulation cells strongly suggests these subpopulations are at least partially distinct from each other and highlights their plasticity during development, with their presence, return and disappearance correlating with changes in the biology of blood cells over the entire lifecourse.

Figure 5. Plasmatocyte subpopulations exhibit distinct localisation and dynamics as adults age

(a-e) representative lateral images of adult flies between 0 and 6 weeks of age showing localisation of cells labelled using *srp-3x-mCherry* (positive control, a), or split GAL4 to drive expression of stinger (*srp-AD;VT-DBD*, b-e). The VT enhancers used to drive expression of the DNA binding domain (*DBD*) of *GAL4* correspond to *VT17559* (b), *VT32897* (c), *VT57089* (d) and *VT62766* (e); inset images show proboscis region at a reduced level of brightness to reveal cellular detail (d). Images contrast enhanced to 0.15% saturation (a-c, e) or 0.75% (d) to reveal localisation of labelled cells due to differing intensities of reporter line expression. Scale bars represent 500μm. At least 5 flies were imaged for each timepoint. See Supplementary Table 1 for full list of genotypes.

Subpopulation cells behave in a functionally-distinct manner compared to the overall plasmatocyte population

Given that the VT lines identified above are specifically and dynamically expressed in subpopulations of hemocytes during *Drosophila* development, we next set out to investigate whether the labelled subpopulations are also functionally distinct using a range of immune-relevant assays. The ability of vertebrate macrophages to respond to pro-inflammatory stimuli, such as injuries, can vary according to their activation status [38,39]. To investigate this in our system, a well-established assay of inflammatory migration [19] was employed (Figure 1a; Supplementary Movie 1). Strikingly, following laser-induced wounding, cells labelled by three *VT-GAL4* lines (*VT17559-GAL4*, *VT32897-GAL4* and *VT62766-GAL4*) showed a significantly more potent migratory response to injury. In each case a greater proportion of labelled subpopulation cells migrated to wounds, compared to the overall hemocyte population as labelled by a pan-plasmatocyte driver (Figure 6a-c). Consistent with our results above, plasmatocytes labelled by the VT lines represent a subset of the total number of hemocytes present ventrally in stage 15 embryos (Figure 6d).

Figure 6. *Drosophila* plasmatocyte subpopulations demonstrate functional differences compared to the overall plasmatocyte population

(a-b) example images showing plasmatocyte wound responses at 60-minutes post-wounding (maximum projection of 15µm deep region). Cells labelled via *UAS-stinger* using *srp-GAL4* (a) and *VT17559-GAL4* (b); dotted lines show wound edges. (c-d) scatterplots showing percentage of *srp-GAL4* (control) or *VT-GAL4* labelled plasmatocytes responding to wounds at 60 minutes (c) or total numbers of labelled plasmatocytes in wounded region (d); p=0.018, 0.041, 0.99, 0.0075 compared to *srp-GAL4* (n=77, 21, 22, 26, 25) (c); p<0.0001 compared to *srp-GAL4* for all lines (n=139, 35, 37, 30, 44) (d). (e-f) example tracks of plasmatocytes labelled with GFP via *srp-GAL4* (e) and *VT17559-GAL4* (f) during random migration on the ventral side of the embryo for 1 hour at stage 15. (g-h) scatterplots showing speed per plasmatocyte, per embryo (g) and directionality (h) at stage 15 in

344 embryos containing cells labelled via *srp-GAL4* (control) or the *VT-GAL4* lines indicated; p=0.0097,
345 0.999, 0.82, 0.226 compared to *srp-GAL4* (n=21, 19, 17, 21, 20) (g); p=0.998, 0.216, 0.480, 0.999
346 compared to *srp-GAL4* (n=21, 19, 17, 21, 20) (h). (i-j) example images of cells on the ventral midline
347 at stage 15 with labelling via *UAS-stinger* expression using *srp-GAL4* (i) and *VT17559-GAL4* (j);
348 zoomed plasmatocytes (i', j') indicated by white boxes in main panels; arrows show vacuoles, "n"
349 marks nucleus; n.b. panels contrast enhanced independently to show plasmatocyte morphology. (k)
350 scatterplots showing vacuoles per plasmatocyte, per embryo at stage 15 (measure of
351 efferocytosis/apoptotic cell clearance); cells labelled via *srp-GAL4* (control) or the *VT-GAL4* lines
352 indicated; p=0.0020, 0.99, 0.0040, 0.0002 compared to *srp-GAL4* (n=76, 10, 12, 29, 31). Lines and
353 error bars represent mean and standard deviation, respectively (all scatterplots); one-way ANOVA
354 with a Dunnett's multiple comparison test used to compare *VT-GAL4* lines with *srp-GAL4* control in
355 all datasets; ns, *, ** and **** denote p>0.05, p<0.05, p<0.01 and p<0.0001, respectively. All scale
356 bars represent 20μm. See Supplementary Table 1 for full list of genotypes.
357
358 We next investigated in vivo migration speeds of the embryonic plasmatocyte subpopulations (as
359 per Figure 1c-d). Stage 15 embryos were imaged for 1 hour and individual plasmatocyte movements
360 were tracked (Figure 6e-f). Only the *VT17559-GAL4* labelled plasmatocyte subpopulation displayed
361 statistically significantly faster rates of migration compared to the overall plasmatocyte population
362 (labelled using *srp-Gal4*; Figure 6g). There were no differences in directionality (cell displacement
363 divided by total path length) for any of the subpopulations, suggesting that the mode of migration
364 was similar across these lines and with that of the overall population (Figure 6h).
365
366 Apoptotic cell clearance (efferocytosis) represents another evolutionarily-conserved function
367 performed by embryonic plasmatocytes (Figure 1e; [40]). Therefore, we investigated this function in
368 subpopulations, using numbers of vacuoles per cell as a proxy for this process [18]. Cells labelled via
369 *VT17559-GAL4*, *VT57089-GAL4* and *VT62766-GAL4* (but not *VT32897-GAL4*) contained fewer

370 vacuoles than the overall plasmatocyte population (Figure 6i-k), suggesting that these discrete
371 populations of cells are less effective at removing apoptotic cells inside the developing embryo.
372
373 Finally, we examined cell size and shape of labelled plasmatocyte subpopulations. Vertebrate
374 macrophages are highly heterogeneous, with distinct morphologies dependent upon their tissue of
375 residence or polarisation status [41–43]. We found no obvious size or shape differences between *VT-*
376 *GAL4* labelled cells and the overall plasmatocyte population (Supplementary Figure 2a-e). This was
377 also the case when *VT-GAL4* positive cells were compared to internal controls (*VT-GAL4* negative
378 cells within the same embryos) for a range of shape descriptors (Supplementary Figure 2f-i).
379 Similarly, we were unable to detect differences in ROS levels or the proportion of *VT-GAL4* labelled
380 plasmatocytes that phagocytosed pHrodo-labelled *E. coli* compared to controls (Supplementary
381 Figures 3 and 4), two processes associated with pro-inflammatory activation of macrophages [44].
382
383 Taken together these data show that the subpopulations of plasmatocytes identified via the *VT-*
384 *GAL4* reporters exhibit functional differences compared to the overall plasmatocyte population
385 (Table 1). Therefore, as well as displaying molecular differences in the form of differential enhancer
386 activity, and hence reporter expression, these discrete populations of cells behave differently. This
387 strongly suggests that these cells represent functionally-distinct subpopulations and that the
388 plasmatocyte lineage is not homogeneous. Furthermore, not all subpopulations displayed identical
389 functional characteristics, suggesting that there are multiple distinct subtypes present in vivo,
390 although some overlap between subpopulations seems likely. For example, *VT17559-GAL4* labelled
391 cells were more effective at responding to wounds and migrated more rapidly, but carried out less
392 phagocytosis of apoptotic cells. By contrast, *VT32987-GAL4* labelled cells only displayed improved
393 wound responses (Figure 6).
394

Table 1. Summary of plasmatocyte subpopulation characteristics and their developmental regulation

VT enhancers identify functionally active genes within plasmatocytes

In the original study that generated the *VT-GAL4* collection, the majority of active enhancer fragments tested were found to control transcription of neighbouring genes [29]. Thus, genes proximal to enhancers that label plasmatocyte subpopulations represent candidate regulators of immune cell function (Table 2; Figure 7a). *VT62766-GAL4* labels a subpopulation of plasmatocytes with enhanced migratory responses to injury (Figure 6) and this enhancer region is found within the genomic interval containing *paralytic* (*para*), which encodes a subunit of a voltage-gated sodium channel [45], and upstream of the 3' end of *calnexin14D* (*cnx14D*) (Figure 7a). *cnx14D* encodes a calcium-binding chaperone protein resident in the endoplasmic reticulum [46]. Alterations in calcium dynamics are associated with clearance of apoptotic cells [47,48] and modulating calcium signalling within plasmatocytes alters their ability to respond to wounds [49]. Therefore, given the association of *cnx14D* with the *VT62766* enhancer and the potential for plasmatocyte behaviours to be modulated by altered calcium dynamics, we examined whether misexpressing *cnx14D* in all plasmatocytes was sufficient to cause these cells to behave more similarly to the *VT62766* subpopulation. Critically, pan-hemocyte expression of *cnx14D* stimulated wound responses with elevated numbers of plasmatocytes responding to injury compared to controls (Figure 7b-c), consistent with the enhanced wound responses of the endogenous *VT62766-GAL4* positive plasmatocyte subpopulation (Figure 6c). This reveals that genes proximal to subpopulation-defining enhancers represent candidate genes in dictating the biology of cells in those subpopulations. More importantly, misexpression of a subpopulation-linked gene promotes a similar behaviour to that subpopulation in the wider plasmatocyte population.

Table 2. VT enhancer region location and neighbouring genes

Figure 7. Misexpression of *cnx14D* improves plasmatocyte inflammatory responses to injury

(a) chromosomal location of the *VT62766-GAL4* enhancer region. Only one transcript is shown for *para*, which possesses multiple splice variants. The *VT62766* region is highlighted in yellow and by an asterisk; *cnx14D* (indicated by magenta arrow) lies within *para*. (b) scatterplot showing numbers of plasmatocytes present at stage 15 on the ventral side of the embryo ahead of wounding in controls and on misexpression of *cnx14D* in all hemocytes using both *srp-GAL4* and *crq-GAL4* (*hc>cnx14D*); n=30 and 38 for control and *hc>cnx14D* embryos, respectively, p=0.670 via Student's t-test. (c) scatterplot of wound responses 60-minutes post-wounding (number of plasmatocytes at wound, normalised for wound area and to control responses); n= 21 and 30 for control and *hc>cnx14D* embryos, respectively; p=0.0328 via Student's t-test. Line and error bars represent mean and standard deviation, respectively (b-c). See Supplementary Table 1 for full list of genotypes.

Plasmatocyte subpopulations can be modulated via exposure to enhanced levels of apoptosis

Having defined functional differences in embryonic plasmatocyte subpopulations and characterised how these populations shift during development and ageing, we sought to identify the processes via which these subpopulations were specified. In vertebrates, a range of stimuli drive macrophage heterogeneity and polarisation [3,4], with apoptotic cells able to polarise macrophages towards anti-inflammatory phenotypes [50,51]. In the developing fly embryo, high apoptotic cell burdens impair wound responses [52,53], consistent with reprogramming of plasmatocytes towards less wound-responsive states. In order to test whether apoptotic cells might regulate plasmatocyte subpopulations, we exposed plasmatocytes to increased levels of apoptosis in vivo. In the

445 developing fly embryo, both glial cells and plasmatocytes contribute to the clearance of apoptotic
446 cells. We, and others, have previously shown that loss of *repo*, a transcription factor required for
447 glial specification [54–56], leads to decreased apoptotic cell clearance by glia [57], and a subsequent
448 challenge of plasmatocytes with increased levels of developmental apoptosis (Figure 8a-b; [53]).
449 Therefore, a *repo* mutant background represents an established model with which to stimulate
450 plasmatocytes with enhanced levels of apoptosis.
451

452 **Figure 8. *Drosophila* plasmatocyte subpopulation identity can be controlled through**
453 **exposure to apoptotic cells**

454 (a-b) maximum projections showing apoptotic cells (via anti-cDCP-1 staining, magenta in merge) and
455 plasmatocytes (via anti-GFP staining, green in merge) at stage 15 on the ventral midline in control
456 and *repo* mutant embryos. (c-g) maximum projections of the ventral midline showing a negative
457 control embryo (c) and embryos containing *VT-GAL4* labelled plasmatocytes at stage 15 in control (d-
458 g) and *repo* mutant embryos (d'-g'). *VT-GAL4* used to drive *UAS-stinger* expression (green) and *srp-*
459 *H2A-3x-mCherry* used to label plasmatocytes (magenta). Arrows and asterisks indicate examples of
460 *VT-GAL4* positive plasmatocytes and non-plasmatocyte cells, respectively; note loss of non-
461 plasmatocyte *VT-GAL4* expression in *repo* mutants versus controls for *VT62766-GAL4*. (h) scatterplot
462 showing percentage of H2A-3x-mCherry positive cells that are also positive for *VT-GAL4* driven
463 Stinger expression in control and *repo* mutant embryos at stage 15. Student's t-test used to show
464 significant difference between controls and *repo* mutants ($p=0.0009$, n=22, 15 for *VT17559-GAL4*
465 lines; $p=0.0017$, n=37, 28 for *VT32897-GAL4* lines; $p=0.0005$, n=25, 14 for *VT57089-GAL4* lines;
466 $p<0.0001$, n=22, 20 for *VT62766-GAL4* lines). Scale bars represent 10μm (a-g); lines and error bars
467 represent mean and standard deviation (h); **, *** and **** denote $p<0.01$, $p<0.001$ and $p<0.0001$,
468 respectively. See Supplementary Table 1 for full list of genotypes.
469

Using *srp-H2A-mCherry* to mark all plasmatocytes within the embryo (Figure 8c), we quantified the proportion of plasmatocytes labelled via *VT-GAL4* transgenes in *repo* mutants compared to controls (Figure 8d-h). Increased exposure to apoptotic death shifted plasmatocytes out of each subpopulation (Figure 8d-h). Subpopulations exhibited differing sensitivities to contact to apoptotic cells, with *VT62766-GAL4* labelled cells undergoing the largest decrease in labelled cells in a *repo* mutant background (Figure 8h). These results therefore reveal a mechanism via which the molecularly and functionally-distinct subpopulations of plasmatocytes we have identified can be manipulated using an evolutionarily-conserved, physiological stimulus (apoptotic cells) relevant to immune cell programming.

Discussion

We have identified molecularly and functionally-distinct subpopulations of *Drosophila* macrophages (plasmatocytes). These subpopulations showed functional differences compared to the overall plasmatocyte population, exhibiting enhanced responses to injury, faster migration rates and reduced rates of apoptotic cell clearance within the developing embryo. These subpopulations are highly plastic with their numbers varying across development, in line with the changing behaviours of *Drosophila* blood cells across the lifecourse. That these discrete populations of plasmatocytes represent bona fide subpopulations is evidenced by the finding that numbers of cells within subpopulations can be manipulated via exposure to enhanced levels of apoptotic cell death in vivo. Furthermore, pan-hemocyte expression of a gene (*cnx14D*) linked to one of the enhancers used to visualise these subpopulations (*VT62766-GAL4*) shifts the behaviour of these cells towards a more wound-responsive state, resembling the behaviour of *VT62766-GAL4* labelled cells. Taken together this data strongly suggests that *Drosophila* blood cell lineages are more complex than previously known.

Vertebrate macrophage lineages show considerable heterogeneity due to the presence of circulating monocytes, a wide variety of tissue resident macrophages and a spectrum of activation states that can be achieved. Whether more simple organisms such as *Drosophila* exhibit heterogeneity within their macrophage-like lineages has been a topic of much discussion and hints in the literature suggest this as a possibility. The ease of extracting larval hemocytes has meant these cells have received more attention than their embryonic counterparts. Braun and colleagues identified heterogeneity in reporter expression within plasmatocytes in an enhancer trap screen, but without associating these with functional differences [58]. Non-uniform expression has also been reported for plasmatocyte genes such as *hemolectin* [59], *hemese*, *nimrod* [60,61], *croquemort* [26], TGF-β family members [26] and the iron transporter *malvolio* [62], though some of these differences are likely due to incomplete differentiation from a pro-hemocyte state [25]. Recent transcriptional profiling approaches via scRNA-seq have suggested the existence of distinct larval blood cell populations in *Drosophila* [27,28]. One study interpreted this data as reflecting different progenitor/differentiation states [27]; another identified a number of potentially different functional groups, including more activated cell populations displaying expression signatures reflective of active Toll and JNK signalling [28]. Our identification of developmentally-regulated subpopulations, coupled with this recent evidence from larvae, points to heterogeneity within the plasmatocyte lineage.

The subpopulations we have identified are almost entirely absent from L3 larvae (the stage used in the aforementioned scRNA-seq studies) and presumably represent additional heterogeneity specific to other developmental stages. It is clear that the biology of *Drosophila* blood cells varies significantly across the lifecourse: for instance plasmatocytes play strikingly different functional roles in embryos and larvae [35,36], shifting from developmental roles to host defence. Additionally, modes of migration to sites of injury are similar in embryos and pupae (directional migration [19,63]), but larval cells are captured from circulation via adhesion [64]. These functional differences are reflected in molecular differences between embryonic and larval blood cells revealed via bulk

521 RNA-seq [28], with reprogramming within larvae potentially explaining why our VT enhancer-
522 labelled subpopulations are absent at that stage. Transcriptional changes are also associated with
523 steroid hormone-mediated signalling in pupae [37], which may drive re-emergence of
524 subpopulations in time for metamorphosis.
525
526 In higher vertebrates, erythro-myeloid precursor/progenitor cells seed the developing embryo to
527 give rise to tissue resident macrophage populations [65–67]. Intriguingly, the localisation of
528 subpopulations in adult flies shows some biases between subpopulation lines and the overall
529 population, hinting at the potential for some degree of tissue residency in *Drosophila*. Hemocytes
530 localise to and/or play specialised roles at a range of tissues including the respiratory epithelia [68],
531 dorsal vessel [69], ovaries [70], wings [71], gut [72] and proventriculus [73]. It is therefore tempting
532 to speculate that particular subpopulations could be recruited or differentiate in situ in order to
533 carry out specific functions.
534
535 Macrophage diversity enables these important innate immune cells to operate in a variety of niches
536 and carry out a wide variety of functions in vertebrates. Our data demonstrate that not all
537 macrophages are equivalent within the developing *Drosophila* embryo, although the enhancers we
538 have used to identify plasmatocyte subpopulations do not correspond to markers used in defining
539 macrophage polarisation or tissue resident populations in an obvious way. Therefore how the
540 subpopulations we have uncovered map onto existing vertebrate paradigms remains an open
541 question. Nonetheless, the subpopulations we have identified could be viewed as a displaying a pro-
542 inflammatory skewing of immune cell behaviours, given their enhanced wound responses, faster
543 rates of migration and decreased efferocytic capacity. Pro-inflammatory macrophages (M1-like) in
544 vertebrates are associated with clearance of pathogens, release of pro-inflammatory cytokines and,
545 most pertinently, initial responses to injury [44]. In contrast, anti-inflammatory macrophages (M2-

546 like) are more allied with tissue development and repair [74] and can display enhanced rates of
547 efferocytosis [75–77].
548
549 Apoptotic cell clearance can promote anti-inflammatory states in vertebrates [78]. Consequently, it
550 is both consistent and compelling that exposure of *Drosophila* plasmatocytes to excessive levels of
551 apoptotic cells dampens their inflammatory responses to injury and rates of migration in the
552 developing embryo [18,52,53] and also shifts cells out of the more wound-responsive and potentially
553 pro-inflammatory subpopulations we have discovered. Other precedents may be apparent in flies
554 with shifts towards aerobic glycolysis occurring during infection [79], similar to those observed in
555 vertebrate polarisation to pro-inflammatory states [80]. Furthermore, TGF-β signalling is associated
556 with promotion of anti-inflammatory characteristics in vertebrates during resolution of inflammation
557 [78] and these molecules can be found in discrete sets of hemocytes on injury and infection in adult
558 flies [26]. Thus, despite significant evolutionary distance between flies and vertebrates, comparable
559 processes and mechanisms may control the behaviours of their innate immune cells.
560
561 We have concentrated on using the VT enhancers as reporters to follow subpopulation behaviour in
562 vivo, however these elements also potentially identify genes required for specific functions
563 associated with each subpopulation. For instance, the *VT17559* enhancer overlaps *Lisencephaly-1*,
564 which has been shown to be expressed in hemocytes [81]. Furthermore, misexpression of *cnx14D*,
565 located proximally to the *VT62766* enhancer, was sufficient to improve overall wound responses,
566 paralleling the behaviour of the *VT62766-GAL4* labelled subpopulation. Cnx14D can bind calcium and
567 therefore potentially modulates calcium signalling within plasmatocytes. Calcium signalling is known
568 to influence wound responses in flies [49] and plays a central role during phagocytosis of apoptotic
569 cells [47,48]. Therefore a molecule such as Cnx14D, which also has a known role in phagocytosis in
570 *Dictyostelium* [82], could help fine-tune the behaviour of specific macrophage subpopulations. When
571 considered in combination with the ability to manipulate the numbers of cells within subpopulations

572 with physiologically relevant stimuli, the functional linkage of candidate genes with subpopulation
573 behaviours strongly suggests that we have identified bona fide functionally and molecularly-distinct
574 macrophage subpopulations in the fly.
575
576 In conclusion, we have demonstrated that *Drosophila* macrophages are a heterogeneous population
577 of cells with distinct functional capabilities. We have characterised novel tools in which to visualise
578 these subpopulations and have used these tools to reveal functional differences between these
579 subpopulations and the general complement of hemocytes. Furthermore, we have shown that these
580 subpopulations can be manipulated by exposure to apoptotic cells and can be linked to specific
581 functional players. Therefore, we have further established *Drosophila* as a model for studying
582 macrophage heterogeneity and immune programming and demonstrate that macrophage
583 heterogeneity is a key feature of the innate immune system even in the absence of adaptive
584 immunity and is conserved more widely across evolution than previously anticipated.
585

586 # Methods

587 ## Fly genetics and reagents

588 Standard cornmeal/agar/molasses media was used to culture *Drosophila* at 25°C (see Supplementary
589 Table 2 for ingredients). *srp-GAL4* [83], *crq-GAL4* [19], *da-GAL4* [84] and the *GAL4*-independent lines
590 *srp-GMA* [30], *srp-3x-mCherry* and *srp-H2A-3xmCherry* [85] were used to label the entire hemocyte
591 population during embryonic development or in adults. *Hml(Δ)-GAL4* was used to label larval
592 hemocytes [86]. *srp-GAL4, Hml(Δ)-GAL4*, *VT-GAL4* lines (obtained from the VDRC, Vienna; [29]) and
593 split GAL4 lines (see below) were used to drive expression from *UAS-tdTomato* (Bloomington stock
594 36327), *UAS-GFP*, *UAS-red stinger*, *UAS-stinger*, *UAS-cnx14D* (Harvard stock d04188) or *UAS-GC3ai*
595 [87]. Experiments were conducted in a w^{1118} background and the $repo^{03702}$ null allele was used to
596 expose plasmatocytes to enhanced levels of apoptotic cell death in the embryo [53,54,56]. Both

UAS-tdTomato and *UAS-GFP* were used to analyse subpopulations in the developing embryo in order to ensure labeling of discrete numbers of plasmatocytes was not due to positional effects of insertion sites that led to mosaic expression (Figure 2). See Supplementary Table 1 for a full list of *Drosophila* genotypes, transgenes and the sources of the *Drosophila* lines used in this study.

Flies were added to laying cages attached to apple juice agar plates supplemented with yeast paste and allowed to acclimatise for 2 days before embryo collection. Plates were then changed every evening and cages incubated at 22°C overnight before embryos were collected the following morning. Embryos were collected by washing the plates with distilled water and gently disturbing the embryos with a paintbrush, after which embryos were collected into a cell strainer. Embryos were dechorionated in undiluted bleach for 1-2 minutes and then washed in distilled water until free from bleach. The fluorescent balancers *CTG*, *CyO dfd*, *TTG* and *TM6b dfd* [88,89] were used to discriminate homozygous embryos after removal of the chorion.

Generation of split GAL4 transgenic lines

We used the split GAL4 system [31] to restrict VT enhancer expression to *serpent*-positive cells. The activation domain (AD) of *GAL4* was expressed using a well-characterised fragment of the hemocyte-specific *serpent* promoter [83,85] and the DNA-binding domain (DBD) was expressed under the control of VT enhancer regions corresponding to *VT17559-GAL4*, *VT32897-GAL4*, *VT57089-GAL4* or *VT62766-GAL4*. High-fidelity polymerase (KAPA HiFi Hotstart ReadyMix, Roche) was used to PCR amplify VT enhancer regions from w^{1118} genomic DNA, which were then TA cloned into the pCR8/GW/TOPO vector. Primers were designed according to VT enhancer sequences available via the Stark Lab Fly Enhancers website (http://enhancers.starklab.org/; [29]). To make *VT-DBD* transgenic constructs, VT enhancers were transferred from *pCR8/GW/TOPO* into *pBPZpGal4DBDUw* (Addgene clone 26233) using LR clonase technology (Invitrogen Gateway LR Clonase II Enzyme Mix - Catalog Number 11791-020).

623

624 To express the *DBD* and *AD* of *GAL4* under the control of the *serpent* promoter (*srp-AD* and *srp-*
625 *DBD*), these were subcloned into an attB containing vector containing this promoter
626 (*pBS_MCS_SRPW_attB*; DSPL337 – a gift from Daria Siekhaus, IST, Austria; [85]). *DBD* and *AD*
627 sequences along with the *Drosophila* synthetic minimal core promoter (DSCP) region were amplified
628 using PCR from vectors *pBPZpGal4DBDUw* and *pBPp65ADZpUw* (Addgene clone 26234) using
629 primers that added NotI and AvrII restriction sites
630 (CTGATCGCGGCCGCAAAGTGGTGATAAACGGCCGGC and
631 GATCAGCCTAGGGTGGATCTAAACGAGTTTTTAAGCAAACTCAC). These were subcloned into DSPL337
632 cut with NotI/AvrII (New England Biolabs) using T4 DNA ligase (Promega). Transgenic flies were
633 generated by site-specific insertion of transgenic constructs into the VK1 attP site on chromosome 2
634 and/or attP2 on chromosome 3 by Genetivision (Texas, USA).
635

636 **Imaging of *Drosophila* embryos, larvae, pupae and adults**

637 Live embryos were mounted ventral-side up on double-sided sticky tape in a minimal volume of
638 Voltalef oil (VWR), after dechorionation in bleach as per Evans et al., 2010 [90]. High-resolution live
639 imaging of plasmatocytes was carried out on an UltraView Spinning Disk system (Perkin Elmer) using
640 a40x UplanSApo oil immersion objective lens (NA 1.3). A Nikon A1 confocal microscope was used to
641 image plasmatocyte morphology (40x CFI Super Plan Fluor ELWD oil immersion objective lens, NA
642 0.6) and a Zeiss Airyscan microscope (40x Plan-Apochromat oil immersion objective lens, NA 1.4)
643 was used for imaging of embryos stained with ROS dyes.
644

645 Wandering L3 Larvae were removed from straight-sided culture bottles containing the food on which
646 they were reared at 25°C and cleaned in distilled water. Larvae were then imaged in fresh ice-cold,
647 distilled water using a MZ205 FA fluorescent dissection microscope with a 2x PLANAPO objective

lens (Leica) and LasX software (Leica). White pre-pupae were collected from the same culture bottles and washed before imaging on the same system, which was also used to image subsequent stages of development. For analysis of plasmatocyte populations in pupae, white pre-pupae were also collected, aged at 25°C and the pupal case removed at a range of times after puparium formation. Dissected pupae were covered with halocarbon oil 500 (Sigma-Aldrich) to prevent desiccation during imaging. For imaging of plasmatocyte populations in adults, females were aged in vials containing cornmeal/agar/molasses media at 25°C, with no more than 7 flies kept per vial. Flies were transferred to new food vials every 2-3 days.

Wounding assay

Live stage 15 embryos were prepared and mounted as described above. The ventral epithelium of the embryos was ablated on the ventral midline using a Micropoint nitrogen-pulsed ablation laser (Andor) fitted to an Ultraview spinning disk confocal system (PerkinElmer) as as per Evans et al., 2015 [91]. Pre-wound z-stacks of 30µm were taken of superficial plasmatocytes with a 1µm z-spacing between z-slices. Post-wound images were taken on the same settings either at 2-minute intervals for 60 minutes (Figure 1) or at the end timepoint of 60 minutes (Figures 6 and 7).

The proportion of plasmatocytes labelled with *UAS-stinger* (expression via *srp-GAL4* or *VT-GAL4*) was assessed by counting the number of labelled cells at or in contact with the wound site within a 35µm deep volume on the ventral midline at 60-minutes post-wounding; this was divided by the total number of labelled cells present within the stack to calculate the percentage of plasmatocytes responding to injury. The brightfield channel was used to visualise the wound margin and only those embryos with wounds between 1000µm^2 and 4000µm^2 were included in analyses. Quantification was performed on blinded images in Fiji.

673 **Quantification of migration speeds/random migration**

674 Embryos were prepared and mounted as described by Evans et al., 2010 [90]. Random migration was
675 imaged using a spinning disk system (Ultraview, PerkinElmer), with an image taken every 2 minutes
676 for 1 hour with a z-spacing of 1µm and approximately 20µm deep from the ventral nerve cord using
677 a 20x UplanSApo air objective lens (NA 0.8). Maximum projections were made for each timepoint
678 (25µm depth) and the centre of individual plasmatocyte cell bodies tracked using the manual
679 tracking plugin in Fiji. Random migration speed (µm/min) and directionality (the ratio of the
680 Cartesian distance to the actual distance migrated) were then calculated using the Ibidi chemotaxis
681 plugin.

682

683 **Quantification of apoptotic cell clearance**

684 The number of vacuoles per plasmatocyte (averaged per embryo) was used as a read-out of
685 apoptotic cell clearance as per Evans et al., 2013 [18]. Vacuoles were counted using z-stacks of GFP-
686 labelled plasmatocytes taken from live imaging experiments. Vacuoles were scored in the z-slice in
687 which each macrophage exhibited its maximal cross-sectional area. Only labelled plasmatocytes
688 present on the ventral midline of stage 15 embryos were included. Analysis was performed on
689 blinded image stacks. This analysis does not report the absolute numbers of apoptotic corpses per
690 cell but provides a relative read-out of the phagocytic index.

691

692 **Fixation and immunostaining of embryos**

693 Embryos were fixed and stained as per Roddie et al., 2019 [52]. Embryos containing plasmatocytes
694 labelled via *srp-GMA* and *GAL4*-driven tdTomato expression were fixed, then mounted in Dabco
695 mountant. Control and *repo* mutant embryos containing plasmatocytes labelled via *crq-GAL4,UAS-*
696 *GFP* were fixed and immunostained using mouse anti-GFP (ab1218 1:200; Abcam) and rabbit anti-
697 cleaved DCP-1 (9578S 1:1000; Cell Signaling Technologies) to detect plasmatocytes and apoptotic
698 cells, respectively. Embryos were imaged on the Nikon A1 system described above.

699

700 **Dissection, culture and stimulation of larval hemocytes**

701 Hemocytes were dissected from wandering L3 larvae by ripping open larvae from the posterior end
702 in S2 cell media, which consists of Schneider's media (Sigma) supplemented with 10% heat-
703 inactivated FBS (Gibco/Sigma) and 1X Pen/Strep (Gibco). 75µl of S2 media was used per larva with
704 multiple larvae pooled per experiment. Cells in suspension were then transferred to glass-bottomed
705 96-well plates (Porvair) and allowed to adhere in a humidified box in the dark for 2 hours ahead of
706 stimulation with heat-killed *S. cerevisiae* particles stained using calcofluor staining solution (Sigma).

707

708 *S. cerevisiae* (strain BY4741/accession number Y00000, Euroscarf consortium) were grown to
709 exponential phase in YPD broth (Fisher) at 28°C. Yeast were heat killed at 60°C for 30 minutes, spun
710 down and frozen at 20 x 10^9 cells/ml. 1x10^9 heat-killed yeast particles in 1ml of PBS (Fluka) were
711 stained for 30 minutes at room temperature (with rotation) using 15µl of calcofluor staining
712 solution. Stained yeast particles were washed in PBS and 1 x 10^6 particles resuspended in 75µl S2 cell
713 medium, which was then added to each well of larval hemocytes for 2 hours. Cells were fixed in
714 wells using 4% EM-grade formaldehyde in PBS for 15 minutes and washed in PBS. Images were taken
715 on a Nikon Ti-E inverted fluorescence microscope using a 20x objective lens and GFP and DAPI filter
716 sets.

717

718 **Image analysis and statistical analysis**

719 All microscopy images were processed using Fiji [92]. Images were typically analysed as maximum z-
720 projections, with the exception of analysis of numbers of cells labelled via *VT-GAL4* lines (Figure 2h),
721 wound responses (Figure 6c-d), vacuolation (Figure 6k) and quantification of ROS staining
722 (Supplementary Figure 3f). Quantification was performed on blinded z-stacks for these analyses.
723 Statistical tests were performed using Prism 7 (GraphPad Software, La Jolla, California, USA). P

values less than 0.05 were deemed significant. A Student's t-test was performed when comparing two sets of parametric data. When multiple comparisons were required, a one-way ANOVA with Dunnett's multiple comparisons test was performed.

Acknowledgements

This work was funded by a Wellcome/Royal Society Sir Henry Dale Fellowship (102503/Z/13/Z) awarded to IRE and a Bateson Centre studentship awarded to IRE, MPZ and JAC. Imaging work was performed at the Wolfson Light Microscopy Facility, using the Perkin Elmer spinning disk (MRC grant G0700091 and Wellcome grant 077544/Z/05/Z), Nikon A1 confocal/TIRF (Wellcome grant WT093134AIA) and Zeiss AiryScan microscopes. This work would not be possible without reagents and resources obtained from or maintained by the Bloomington *Drosophila* Stock Centre (NIH P40OD018537), the Vienna *Drosophila* Research Centre and Flybase (NIH and MRC grants U41 HG000739 and MR/N030117/1, respectively). We thank the *Drosophila* community for sharing *Drosophila* reagents (see Supplementary Table 1). We are grateful to Darren Robinson and the Fly Facility staff (University of Sheffield) for their support and to Phil Elks and Simon Johnston (University of Sheffield) for critical reading and feedback on the manuscript. We particularly thank Phil Elks and the now sadly departed Jarema Malicki for their advice and suggestions throughout the project. We thank Agata Grettka and Eleanor Castle for additional experiments that have contributed to our understanding of this project.

Author contributions

Experiments performed by JAC, AB, ELA and IRE. JAC, AB and IRE wrote the initial manuscript. All authors contributed to experimental design and revision of the manuscript. The project was conceived and funding obtained by IRE and MZ.

Declaration of interests

The authors declare no competing interests.

References

1. Wynn TA, Chawla A, Pollard JW. Macrophage biology in development, homeostasis and disease. Nature. 2013. doi:10.1038/nature12034

2. Gordon S, Plüddemann A. Tissue macrophages: heterogeneity and functions. BMC Biol. BioMed Central; 2017;15: 53. doi:10.1186/s12915-017-0392-4

3. Martinez FO, Gordon S. The M1 and M2 paradigm of macrophage activation: time for reassessment. F1000Prime Rep. 2014;6. doi:10.12703/P6-13

4. Murray PJ. Macrophage Polarization. Annu Rev Physiol. 2017; doi:10.1146/annurev-physiol-022516-034339

5. Nguyen-Chi M, Laplace-Builhe B, Travnickova J, Luz-Crawford P, Tejedor G, Phan QT, et al. Identification of polarized macrophage subsets in zebrafish. Elife. 2015;4: e07288. doi:10.7554/eLife.07288

6. Xu J, Wang T, Wu Y, Jin W, Wen Z. Microglia Colonization of Developing Zebrafish Midbrain Is Promoted by Apoptotic Neuron and Lysophosphatidylcholine. Dev Cell. 2016;38: 214–22. doi:10.1016/j.devcel.2016.06.018

7. Ferrero G, Mahony CB, Dupuis E, Yvernogeau L, Di Ruggiero E, Miserocchi M, et al. Embryonic Microglia Derive from Primitive Macrophages and Are Replaced by cmyb-Dependent Definitive Microglia in Zebrafish. Cell Rep. 2018; doi:10.1016/j.celrep.2018.05.066

8. Wiegertjes GF, Wentzel AS, Spaink HP, Elks PM, Fink IR. Polarization of immune responses in

fish: The 'macrophages first' point of view. Mol Immunol. 2016; doi:10.1016/j.molimm.2015.09.026

9. Buchmann K. Evolution of innate immunity: Clues from invertebrates via fish to mammals. Front Immunol. 2014; doi:10.3389/fimmu.2014.00459

10. Murray PJ, Wynn TA. Protective and pathogenic functions of macrophage subsets. Nat Rev Immunol. 2011;11: 723–737. doi:10.1038/nri3073

11. Murray PJ, Allen JE, Biswas SK, Fisher EA, Gilroy DW, Goerdt S, et al. Macrophage Activation and Polarization: Nomenclature and Experimental Guidelines. Immunity. 2014. doi:10.1016/j.immuni.2014.06.008

12. Colin S, Chinetti-Gbaguidi G, Staels B. Macrophage phenotypes in atherosclerosis. Immunol Rev. John Wiley & Sons, Ltd; 2014;262: 153–166. doi:10.1111/imr.12218

13. Vogel DYS, Glim JE, Stavenuiter AWD, Breur M, Heijnen P, Amor S, et al. Human macrophage polarization in vitro: Maturation and activation methods compared. Immunobiology. 2014;219: 695–703. doi:10.1016/j.imbio.2014.05.002

14. Buchon N, Silverman N, Cherry S. Immunity in Drosophila melanogaster — from microbial recognition to whole-organism physiology. Nat Rev Immunol. 2014;14: 796–810. doi:10.1038/nri3763

15. Evans CJ, Hartenstein V, Banerjee U. Thicker than blood: conserved mechanisms in Drosophila and vertebrate hematopoiesis. Dev Cell. 2003;5: 673–90. Available: http://www.ncbi.nlm.nih.gov/pubmed/14602069

16. Wood W, Jacinto A. Drosophila melanogaster embryonic haemocytes: masters of multitasking. Nat Rev Mol Cell Biol. Nature Publishing Group; 2007;8: 542–551. doi:10.1038/nrm2202

17. Ratheesh A, Belyaeva V, Siekhaus DE. Drosophila immune cell migration and adhesion during embryonic development and larval immune responses. Current Opinion in Cell Biology. 2015. pp. 71–79. doi:10.1016/j.ceb.2015.07.003

798 18. Evans IR, Ghai PA, Urbančič V, Tan KL, Wood W. SCAR/WAVE-mediated processing of
799 engulfed apoptotic corpses is essential for effective macrophage migration in Drosophila. Cell
800 Death Differ. 2013;20: 709–720. doi:10.1038/cdd.2012.166
801 19. Stramer B, Wood W, Galko MJ, Redd MJ, Jacinto A, Parkhurst SM, et al. Live imaging of
802 wound inflammation in Drosophila embryos reveals key roles for small GTPases during in vivo
803 cell migration. J Cell Biol. 2005;168: 567–573. doi:10.1083/jcb.200405120
804 20. Paladi M, Tepass U. Function of Rho GTPases in embryonic blood cell migration in Drosophila.
805 J Cell Sci. 2004;117: 6313–26. doi:10.1242/jcs.01552
806 21. Siekhaus D, Haesemeyer M, Moffitt O, Lehmann R. RhoL controls invasion and Rap1
807 localization during immune cell transmigration in Drosophila. Nat Cell Biol. 2010;
808 doi:10.1038/ncb2063
809 22. Comber K, Huelsmann S, Evans I, Sanchez-Sanchez BJ, Chalmers A, Reuter R, et al. A dual role
810 for the PS integrin myospheroid in mediating Drosophila embryonic macrophage migration. J
811 Cell Sci. 2013;126: 3475–3484. doi:10.1242/jcs.129700
812 23. Manaka J, Kuraishi T, Shiratsuchi A, Nakai Y, Higashida H, Henson P, et al. Draper-mediated
813 and phosphatidylserine-independent phagocytosis of apoptotic cells by Drosophila
814 hemocytes/macrophages. J Biol Chem. 2004;279: 48466–48476.
815 doi:10.1074/jbc.M408597200
816 24. Franc NC, Dimarcq JL, Lagueux M, Hoffmann J, Ezekowitz RAB. Croquemort, a novel
817 drosophila hemocyte/macrophage receptor that recognizes apoptotic cells. Immunity.
818 1996;4: 431–443. doi:10.1016/S1074-7613(00)80410-0
819 25. Banerjee U, Girard JR, Goins LM, Spratford CM. *Drosophila* as a Genetic Model for
820 Hematopoiesis. Genetics. 2019;211: 367–417. doi:10.1534/genetics.118.300223
821 26. Clark RI, Woodcock KJ, Geissmann F, Trouillet C, Dionne MS. Multiple TGF-β superfamily
822 signals modulate the adult drosophila immune response. Curr Biol. 2011;21: 1672–1677.
823 doi:10.1016/j.cub.2011.08.048

824 27. Tattikota SG, Hu Y, Liu Y, Cho B, Barrera V, Steinbaugh M, et al. A single-cell survey of
825 Drosophila blood. bioRxiv. Cold Spring Harbor Laboratory; 2019; 2019.12.20.884999.
826 doi:10.1101/2019.12.20.884999
827 28. Cattenoz PB, Sakr R, Pavlidaki A, Delaporte C, Riba A, Molina N, et al. Temporal specificity and
828 heterogeneity of *Drosophila* immune cells. EMBO J. 2020; e104486.
829 doi:10.15252/embj.2020104486
830 29. Kvon EZ, Kazmar T, Stampfel G, Yáñez-Cuna JO, Pagani M, Schernhuber K, et al. Genome-scale
831 functional characterization of Drosophila developmental enhancers in vivo. Nature. 2014;
832 doi:10.1038/nature13395
833 30. Dutta D, Bloor JW, Ruiz-Gomez M, VijayRaghavan K, Kiehart DP. Real-time imaging of
834 morphogenetic movements indrosophila using Gal4-UAS-driven expression of GFP fused to
835 the actin-binding domain of moesin. genesis. 2002;34: 146–151. doi:10.1002/gene.10113
836 31. Pfeiffer BD, Ngo T-TB, Hibbard KL, Murphy C, Jenett A, Truman JW, et al. Refinement of Tools
837 for Targeted Gene Expression in Drosophila. Genetics. 2010;186: 735–755.
838 doi:10.1534/genetics.110.119917
839 32. Lebestky T, Chang T, Hartenstein V, Banerjee U. Specification of Drosophila Hematopoietic
840 Lineage by Conserved Transcription Factors. Science (80-). 2000;288: 146–149.
841 doi:10.1126/science.288.5463.146
842 33. Brodu R, Mugat B, Roignant J-Y, Lepesant J-A, Antoniewski C. Dual Requirement for the
843 EcR/USP Nuclear Receptor and the dGATAb Factor in an Ecdysone Response in Drosophila
844 melanogaster [Internet]. MOLECULAR AND CELLULAR BIOLOGY. 1999. Available:
845 http://mcb.asm.org/
846 34. Das D, Ashoka D, Aradhya R, Inamdar M. Gene expression analysis in post-embryonic
847 pericardial cells of Drosophila. Gene Expr Patterns. Elsevier; 2008;8: 199–205.
848 doi:10.1016/J.GEP.2007.10.008
849 35. Charroux B, Royet J. Elimination of plasmatocytes by targeted apoptosis reveals their role in

multiple aspects of the Drosophila immune response. Proc Natl Acad Sci U S A. 2009; doi:10.1073/pnas.0903971106

36. Defaye A, Evans I, Crozatier M, Wood W, Lemaitre B, Leulier F. Genetic ablation of Drosophila phagocytes reveals their contribution to both development and resistance to bacterial infection. J Innate Immun. 2009;1: 322–334.

37. Regan JC, Brandão AS, Leitão AB, Mantas Dias ÂR, Sucena É, Jacinto A, et al. Steroid Hormone Signaling Is Essential to Regulate Innate Immune Cells and Fight Bacterial Infection in Drosophila. PLoS Pathog. 2013;9. doi:10.1371/journal.ppat.1003720

38. Dal-Secco D, Wang J, Zeng Z, Kolaczkowska E, Wong CHY, Petri B, et al. A dynamic spectrum of monocytes arising from the in situ reprogramming of CCR2+ monocytes at a site of sterile injury. J Exp Med. The Rockefeller University Press; 2015;212: 447. doi:10.1084/JEM.20141539

39. Arnold L, Henry A, Poron F, Baba-Amer Y, van Rooijen N, Plonquet A, et al. Inflammatory monocytes recruited after skeletal muscle injury switch into antiinflammatory macrophages to support myogenesis. J Exp Med. The Rockefeller University Press; 2007;204: 1057–69. doi:10.1084/jem.20070075

40. Melcarne C, Lemaitre B, Kurant E. Phagocytosis in Drosophila: From molecules and cellular machinery to physiology. Insect Biochem Mol Biol. Pergamon; 2019;109: 1–12. doi:10.1016/J.IBMB.2019.04.002

41. McWhorter FY, Wang T, Nguyen P, Chung T, Liu WF. Modulation of macrophage phenotype by cell shape. Proc Natl Acad Sci U S A. 2013; doi:10.1073/pnas.1308887110

42. Ploeger DT, Hosper NA, Schipper M, Koerts JA, de Rond S, Bank RA. Cell plasticity in wound healing: paracrine factors of M1/ M2 polarized macrophages influence the phenotypical state of dermal fibroblasts. Cell Commun Signal. 2013;11: 29. doi:10.1186/1478-811X-11-29

43. Rostam HM, Reynolds PM, Alexander MR, Gadegaard N, Ghaemmaghami AM. Image based Machine Learning for identification of macrophage subsets. Sci Rep. Nature Publishing Group;

2017;7: 3521. doi:10.1038/s41598-017-03780-z

44. Benoit M, Desnues B, Mege J-L. Macrophage Polarization in Bacterial Infections. J Immunol. 2008;181: 3733–3739. doi:10.4049/jimmunol.181.6.3733

45. Lin W-H, Wright DE, Muraro NI, Baines RA. Alternative Splicing in the Voltage-Gated Sodium Channel DmNa $_{v}$ Regulates Activation, Inactivation, and Persistent Current. J Neurophysiol. 2009;102: 1994–2006. doi:10.1152/jn.00613.2009

46. Christodoulou S, Lockyer AE, Foster JM, Hoheisel JD, Roberts DB. Nucleotide sequence of a Drosophila melanogaster cDNA encoding a calnexin homologue. Gene. 1997;191: 143–8. doi:10.1016/s0378-1119(97)00025-5

47. Cuttell L, Vaughan A, Silva E, Escaron CJ, Lavine M, Van Goethem E, et al. Undertaker, a Drosophila Junctophilin, Links Draper-Mediated Phagocytosis and Calcium Homeostasis. Cell. 2008;135: 524–534. doi:10.1016/j.cell.2008.08.033

48. Gronski MA, Kinchen JM, Juncadella IJ, Franc NC, Ravichandran KS. An essential role for calcium flux in phagocytes for apoptotic cell engulfment and the anti-inflammatory response. Cell Death Differ. 2009;16: 1323–31. doi:10.1038/cdd.2009.55

49. Weavers H, Evans IR, Martin P, Wood W. Corpse Engulfment Generates a Molecular Memory that Primes the Macrophage Inflammatory Response. Cell. 2016;165. doi:10.1016/j.cell.2016.04.049

50. A-Gonzalez N, Quintana JA, García-Silva S, Mazariegos M, González de la Aleja A, Nicolás-Ávila JA, et al. Phagocytosis imprints heterogeneity in tissue-resident macrophages. J Exp Med. 2017;214: 1281–1296. doi:10.1084/jem.20161375

51. Fulco T de O, Andrade PR, Barbosa MG de M, Pinto TGT, Ferreira PF, Ferreira H, et al. Effect of apoptotic cell recognition on macrophage polarization and mycobacterial persistence. Infect Immun. 2014; doi:10.1128/IAI.02194-14

52. Roddie HG, Armitage EL, Coates JA, Johnston SA, Evans IR. Simu-dependent clearance of dying cells regulates macrophage function and inflammation resolution. PLoS Biol. 2019;

902 doi:10.1371/journal.pbio.2006741

903 53. Armitage EL, Roddie HG, Evans IR. Overexposure to apoptosis via disrupted glial specification
904 perturbs Drosophila macrophage function and reveals roles of the CNS during injury. bioRxiv.
905 Cold Spring Harbor Laboratory; 2020; 2020.03.04.977546. doi:10.1101/2020.03.04.977546

906 54. Campbell G, Göring H, Lin T, Spana E, Andersson S, Doe CQ, et al. RK2, a glial-specific
907 homeodomain protein required for embryonic nerve cord condensation and viability in
908 Drosophila. Development. 1994;120: 2957–66. Available:
909 http://www.ncbi.nlm.nih.gov/pubmed/7607085

910 55. Xiong WC, Okano H, Patel NH, Blendy JA, Montell C. repo encodes a glial-specific homeo
911 domain protein required in the Drosophila nervous system. Genes Dev. 1994;
912 doi:10.1101/gad.8.8.981

913 56. Halter D a, Urban J, Rickert C, Ner SS, Ito K, Travers a a, et al. The homeobox gene repo is
914 required for the differentiation and maintenance of glia function in the embryonic nervous
915 system of Drosophila melanogaster. Development. 1995;121: 317–332.

916 57. Shlyakhover E, Shklyar B, Hakim-Mishnaevski K, Levy-Adam F, Kurant E. Drosophila GATA
917 factor serpent establishes phagocytic ability of embryonic macrophages. Front Immunol.
918 2018; doi:10.3389/fimmu.2018.00266

919 58. Braun A, Lemaitre B, Lanot R, Zachary D, Meister M. Drosophila immunity: analysis of larval
920 hemocytes by P-element-mediated enhancer trap. Genetics. Genetics Society of America;
921 1997;147: 623–34. Available: http://www.ncbi.nlm.nih.gov/pubmed/9335599

922 59. Goto A, Kadowaki T, Kitagawa Y. Drosophila hemolectin gene is expressed in embryonic and
923 larval hemocytes and its knock down causes bleeding defects. Dev Biol. Academic Press;
924 2003;264: 582–591. doi:10.1016/J.YDBIO.2003.06.001

925 60. Kurucz E, Váczi B, Márkus R, Laurinyecz B, Vilmos P, Zsámboki J, et al. Definition of Drosophila
926 hemocyte subsets by cell-type specific antigens. Acta Biol Hung. 2007;58 Suppl: 95–111.
927 doi:10.1556/ABiol.58.2007.Suppl.8

928 61. Kurucz É, Márkus R, Zsámboki J, Folkl-Medzihradszky K, Darula Z, Vilmos P, et al. Nimrod, a
929 Putative Phagocytosis Receptor with EGF Repeats in Drosophila Plasmatocytes. Curr Biol. Cell
930 Press; 2007;17: 649–654. doi:10.1016/J.CUB.2007.02.041
931 62. Folwell JL, Barton CH, Shepherd D. Immunolocalisation of the D. melanogaster Nramp
932 homologue Malvolio to gut and Malpighian tubules provides evidence that Malvolio and
933 Nramp2 are orthologous. J Exp Biol. 2006;209: 1988–1995. doi:10.1242/jeb.02193
934 63. Moreira CGA, Regan JC, Zaidman-Rémy A, Jacinto A, Prag S. Drosophila Hemocyte Migration:
935 An In Vivo Assay for Directional Cell Migration. Methods in molecular biology (Clifton, NJ).
936 2011. pp. 249–260. doi:10.1007/978-1-61779-207-6_17
937 64. Babcock DT, Brock AR, Fish GS, Wang Y, Perrin L, Krasnow M a, et al. Circulating blood cells
938 function as a surveillance system for damaged tissue in Drosophila larvae. Proc Natl Acad Sci
939 U S A. 2008;105: 10017–10022. doi:10.1073/pnas.0709951105
940 65. Mass E, Ballesteros I, Farlik M, Halbritter F, Günther P, Crozet L, et al. Specification of tissue-
941 resident macrophages during organogenesis. Science (80-). 2016;353: aaf4238–aaf4238.
942 doi:10.1126/science.aaf4238
943 66. Gomez Perdiguero E, Klapproth K, Schulz C, Busch K, Azzoni E, Crozet L, et al. Tissue-resident
944 macrophages originate from yolk-sac-derived erythro-myeloid progenitors. Nature. 2015;518:
945 547–551. doi:10.1038/nature13989
946 67. Hoeffel G, Ginhoux F. Fetal monocytes and the origins of tissue-resident macrophages. Cell
947 Immunol. 2018;330: 5–15. doi:10.1016/j.cellimm.2018.01.001
948 68. Sanchez Bosch P, Makhijani K, Herboso L, Gold KS, Baginsky R, Woodcock KJ, et al. Adult
949 Drosophila Lack Hematopoiesis but Rely on a Blood Cell Reservoir at the Respiratory Epithelia
950 to Relay Infection Signals to Surrounding Tissues. Dev Cell. 2019;51: 787-803.e5.
951 doi:10.1016/j.devcel.2019.10.017
952 69. Cevik D, Acker M, Michalski C, Jacobs JR. Pericardin, a Drosophila collagen, facilitates
953 accumulation of hemocytes at the heart. Dev Biol. 2019;454: 52–65.

954 doi:10.1016/j.ydbio.2019.06.006

955 70. Van De Bor V, Zimniak G, Papone L, Cerezo D, Malbouyres M, Juan T, et al. Companion Blood
956 Cells Control Ovarian Stem Cell Niche Microenvironment and Homeostasis. Cell Rep. 2015;13:
957 546–560. doi:10.1016/j.celrep.2015.09.008

958 71. Kiger JA, Natzle JE, Green MM. Hemocytes are essential for wing maturation in Drosophila
959 melanogaster. Proc Natl Acad Sci U S A. 2001;98: 10190–5. doi:10.1073/pnas.181338998

960 72. Ayyaz A, Li H, Jasper H. Haemocytes control stem cell activity in the Drosophila intestine. Nat
961 Cell Biol. 2015;17: 736–748. doi:10.1038/ncb3174

962 73. Zaidman-Rémy A, Regan JC, Brandão AS, Jacinto A. The Drosophila larva as a tool to study
963 gut-associated macrophages: PI3K regulates a discrete hemocyte population at the
964 proventriculus. Dev Comp Immunol. 2012;36: 638–47. doi:10.1016/j.dci.2011.10.013

965 74. Krzyszczyk P, Schloss R, Palmer A, Berthiaume F. The role of macrophages in acute and
966 chronic wound healing and interventions to promote pro-wound healing phenotypes.
967 Frontiers in Physiology. 2018. doi:10.3389/fphys.2018.00419

968 75. Zizzo G, Hilliard BA, Monestier M, Cohen PL. Efficient Clearance of Early Apoptotic Cells by
969 Human Macrophages Requires M2c Polarization and MerTK Induction. J Immunol. 2012;189:
970 3508–3520. doi:10.4049/jimmunol.1200662

971 76. Lingnau M, Höflich C, Volk H-D, Sabat R, Döcke W-D. Interleukin-10 enhances the CD14-
972 dependent phagocytosis of bacteria and apoptotic cells by human monocytes. Hum Immunol.
973 2007;68: 730–738. doi:10.1016/j.humimm.2007.06.004

974 77. Ogden CA, Pound JD, Batth BK, Owens S, Johannessen I, Wood K, et al. Enhanced Apoptotic
975 Cell Clearance Capacity and B Cell Survival Factor Production by IL-10-Activated
976 Macrophages: Implications for Burkitt's Lymphoma. J Immunol. 2005;174: 3015–3023.
977 doi:10.4049/jimmunol.174.5.3015

978 78. Fadok VA, Bratton DL, Konowal A, Freed PW, Westcott JY, Henson PM. Macrophages that
979 have ingested apoptotic cells in vitro inhibit proinflammatory cytokine production through

980 autocrine/paracrine mechanisms involving TGF-beta, PGE2, and PAF. J Clin Invest. 1998;101:
981 890–898. doi:10.1172/JCI1112
982 79. Krejčová G, Danielová A, Nedbalová P, Kazek M, Strych L, Chawla G, et al. Drosophila
983 macrophages switch to aerobic glycolysis to mount effective antibacterial defense. Elife.
984 2019;8. doi:10.7554/eLife.50414
985 80. Van den Bossche J, O'Neill LA, Menon D. Macrophage Immunometabolism: Where Are We
986 (Going)? Trends in Immunology. 2017. doi:10.1016/j.it.2017.03.001
987 81. Williams MJ. The Drosophila cell adhesion molecule Neuroglian regulates Lissencephaly-1
988 localisation in circulating immunosurveillance cells. BMC Immunol. 2009;10: 17.
989 doi:10.1186/1471-2172-10-17
990 82. Muller-Taubenberger A, Lupas AN, Li H, Ecke M, Simmeth E, Gerisch G. Calreticulin and
991 calnexin in the endoplasmic reticulum are important for phagocytosis. EMBO J. 2001;20:
992 6772–6782. doi:10.1093/emboj/20.23.6772
993 83. Brückner K, Kockel L, Duchek P, Luque CM, Rørth P, Perrimon N. The PDGF/VEGF receptor
994 controls blood cell survival in Drosophila. Dev Cell. 2004;7: 73–84.
995 doi:10.1016/j.devcel.2004.06.007
996 84. Wodarz A, Hinz U, Engelbert M, Knust E. Expression of crumbs confers apical character on
997 plasma membrane domains of ectodermal epithelia of drosophila. Cell. 1995;82: 67–76.
998 doi:10.1016/0092-8674(95)90053-5
999 85. Gyoergy A, Roblek M, Ratheesh A, Valoskova K, Belyaeva V, Wachner S, et al. Tools Allowing
1000 Independent Visualization and Genetic Manipulation of *Drosophila melanogaster*
1001 Macrophages and Surrounding Tissues. G3: Genes|Genomes|Genetics. 2018;8:
1002 g3.300452.2017. doi:10.1534/g3.117.300452
1003 86. Sinenko SA, Mathey-Prevot B. Increased expression of Drosophila tetraspanin, Tsp68C,
1004 suppresses the abnormal proliferation of ytr-deficient and Ras/Raf-activated hemocytes.
1005 Oncogene. Nature Publishing Group; 2004;23: 9120–9128. doi:10.1038/sj.onc.1208156

87. Schott S, Ambrosini A, Barbaste A, Benassayag C, Gracia M, Proag A, et al. A fluorescent toolkit for spatiotemporal tracking of apoptotic cells in living *Drosophila* tissues. Development. 2017; dev.149807. doi:10.1242/dev.149807

88. Halfon MS, Gisselbrecht S, Lu J, Estrada B, Keshishian H, Michelson AM. New fluorescent protein reporters for use with the Drosophila Gal4 expression system and for vital detection of balancer chromosomes. Genesis. 2002;34: 135–138. doi:10.1002/gene.10136

89. Le T, Liang Z, Patel H, Yu MH, Sivasubramaniam G, Slovitt M, et al. A New Family of Drosophila Balancer Chromosomes With a w- dfd-GMR Yellow Fluorescent Protein Marker. Genetics. 2006;174: 2255–2257. doi:10.1534/genetics.106.063461

90. Evans IR, Hu N, Skaer H, Wood W. Interdependence of macrophage migration and ventral nerve cord development in Drosophila embryos. Development. 2010;137: 1625–1633. doi:10.1242/dev.046797

91. Evans IR, Rodrigues FSLM, Armitage EL, Wood W. Draper/CED-1 Mediates an Ancient Damage Response to Control Inflammatory Blood Cell Migration In Vivo. Curr Biol. The Authors; 2015;25: 1606–12. doi:10.1016/j.cub.2015.04.037

92. Schindelin J, Arganda-Carreras I, Frise E, Kaynig V, Longair M, Pietzsch T, et al. Fiji: an open-source platform for biological-image analysis. Nat Methods. Nature Publishing Group; 2012;9: 676–682. doi:10.1038/nmeth.2019

Figure 1

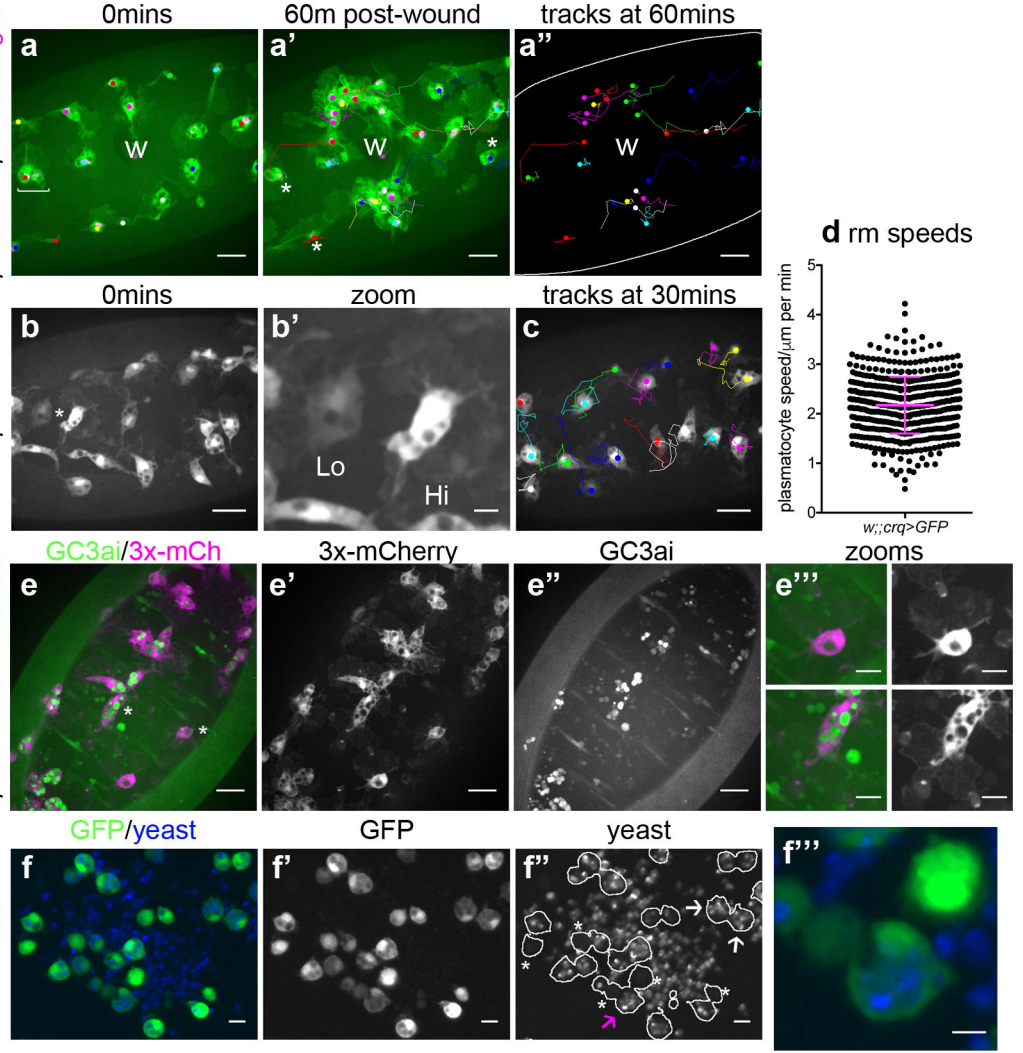
0mins
60m post-wound
tracks at 60mins
srp>GFP/srp>red stinger
a
a'
a''
W
0mins
zoom
tracks at 30mins
crq>GFP
b
b'
c
Lo
Hi
d rm speeds
plasmatocyte speed/μm per min
w;;crq>GFP
GC3ai/3x-mCh
3x-mCherry
GC3ai
zooms
srp-3x-mCh/da>GC3ai
e
e'
e''
e'''
GFP/yeast
GFP
yeast
hml>GFP
f
f'
f''
f'''

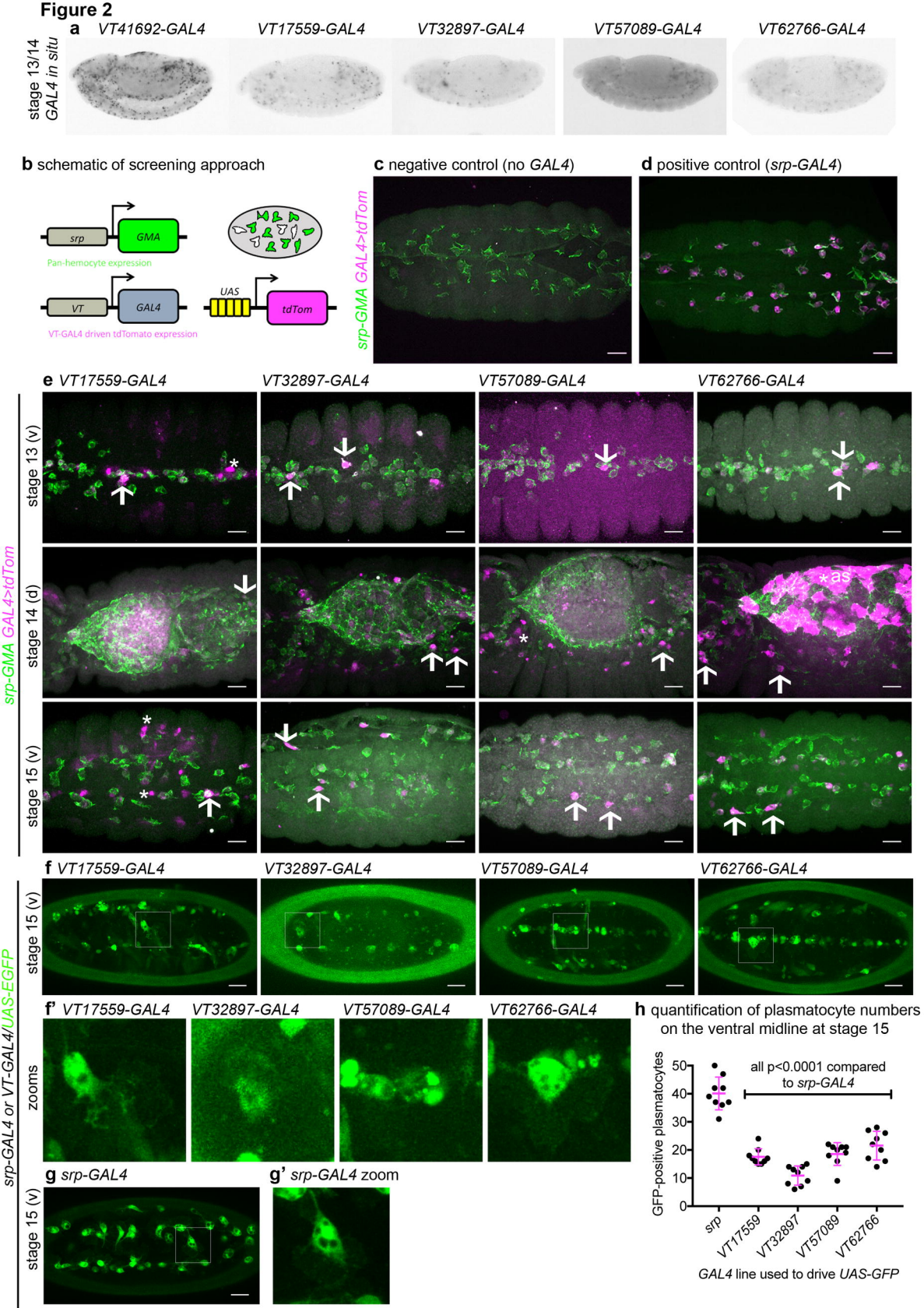
Figure 2
a
VT41692-GAL4
VT17559-GAL4
VT32897-GAL4
VT57089-GAL4
VT62766-GAL4
stage 13/14
GAL4 in situ
b schematic of screening approach
srp
GMA
Pan-hemocyte expression
VT
GAL4
UAS
tdTom
VT-GAL4 driven tdTomato expression
c negative control (no GAL4)
d positive control (srp-GAL4)
srp-GMA GAL4>tdTom
e VT17559-GAL4
VT32897-GAL4
VT57089-GAL4
VT62766-GAL4
stage 13 (v)
stage 14 (d)
stage 15 (v)
*as
srp-GMA GAL4>tdTom
f VT17559-GAL4
VT32897-GAL4
VT57089-GAL4
VT62766-GAL4
stage 15 (v)
f' VT17559-GAL4
VT32897-GAL4
VT57089-GAL4
VT62766-GAL4
zooms
srp-GAL4 or VT-GAL4/UAS-EGFP
g srp-GAL4
g' srp-GAL4 zoom
stage 15 (v)
h quantification of plasmatocyte numbers on the ventral midline at stage 15
all p<0.0001 compared to srp-GAL4
GFP-positive plasmatocytes
0
10
20
30
40
50
srp
VT17559
VT32897
VT57089
VT62766
GAL4 line used to drive UAS-GFP

Figure 3

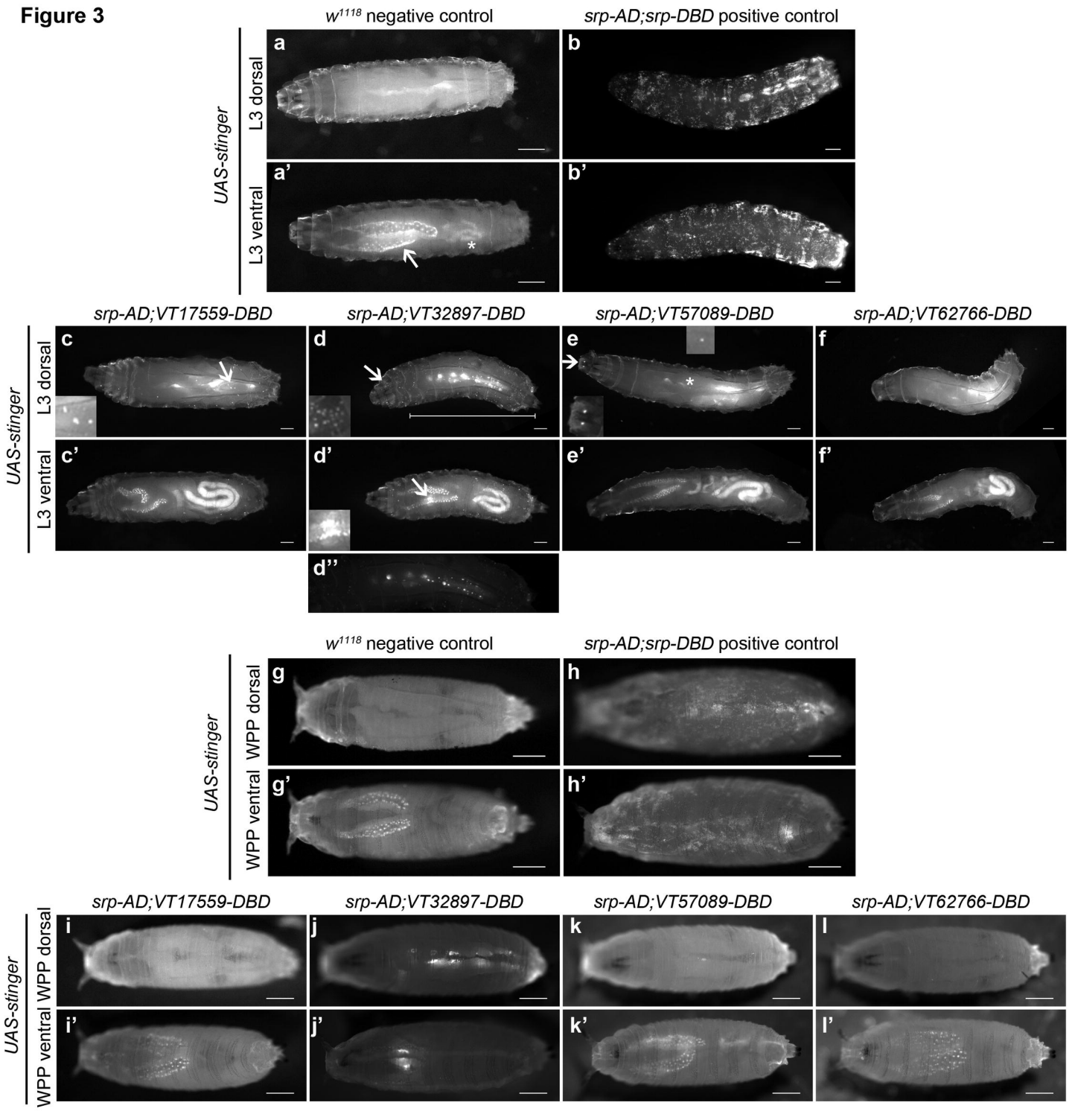
w1118 negative control
srp-AD;srp-DBD positive control
UAS-stinger
L3 dorsal
L3 ventral
a
b
a'
b'
srp-AD;VT17559-DBD
srp-AD;VT32897-DBD
srp-AD;VT57089-DBD
srp-AD;VT62766-DBD
c
d
e
f
c'
d'
e'
f'
d''
WPP dorsal
WPP ventral
g
h
g'
h'
i
j
k
l
i'
j'
k'
l'

Figure 4

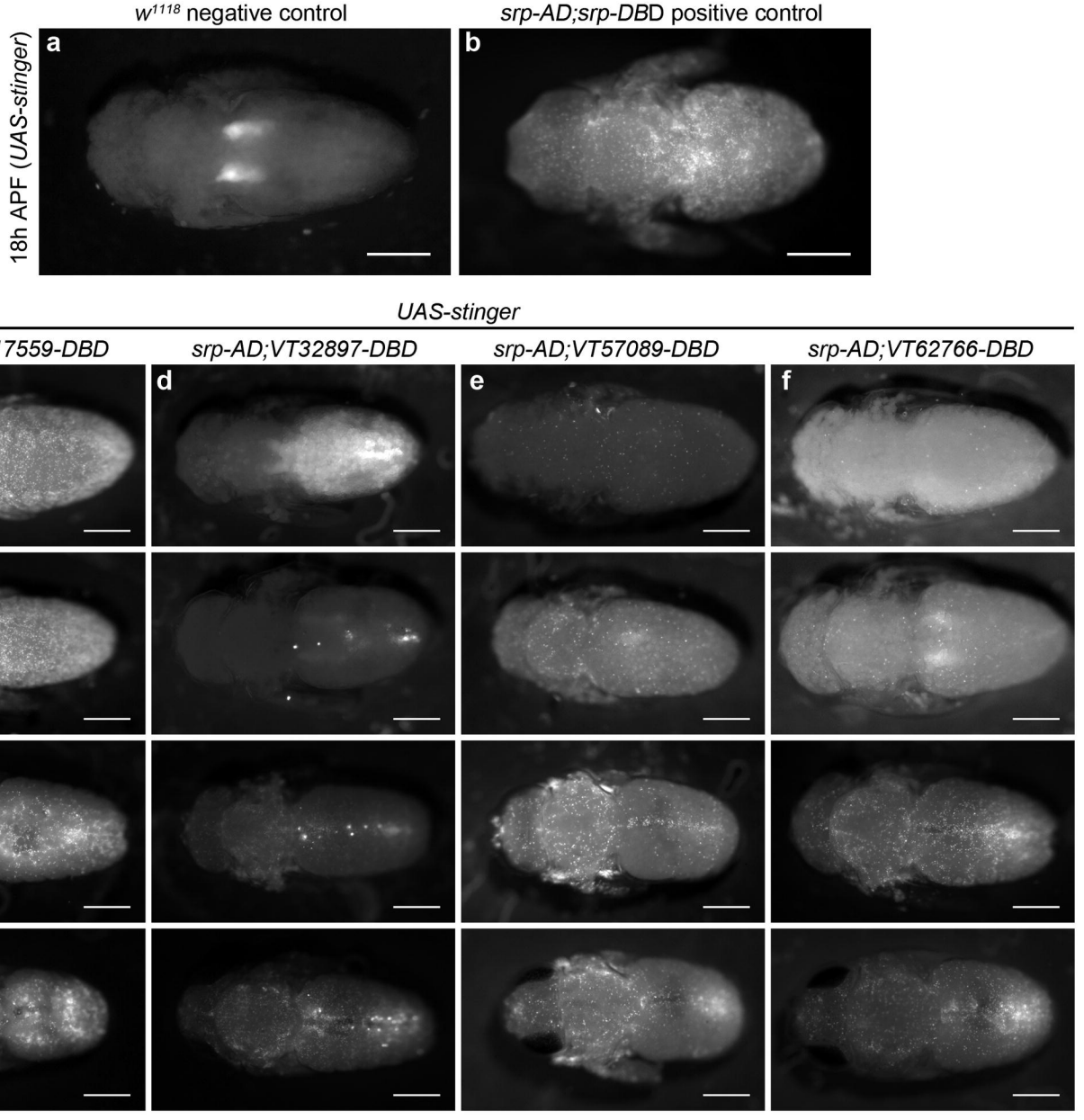
w1118 negative control
srp-AD;srp-DBD positive control
18h APF (UAS-stinger)
a
b
UAS-stinger
srp-AD;VT17559-DBD
srp-AD;VT32897-DBD
srp-AD;VT57089-DBD
srp-AD;VT62766-DBD
c
d
e
f
18h APF
24h APF
48h APF
72h APF

Figure 5

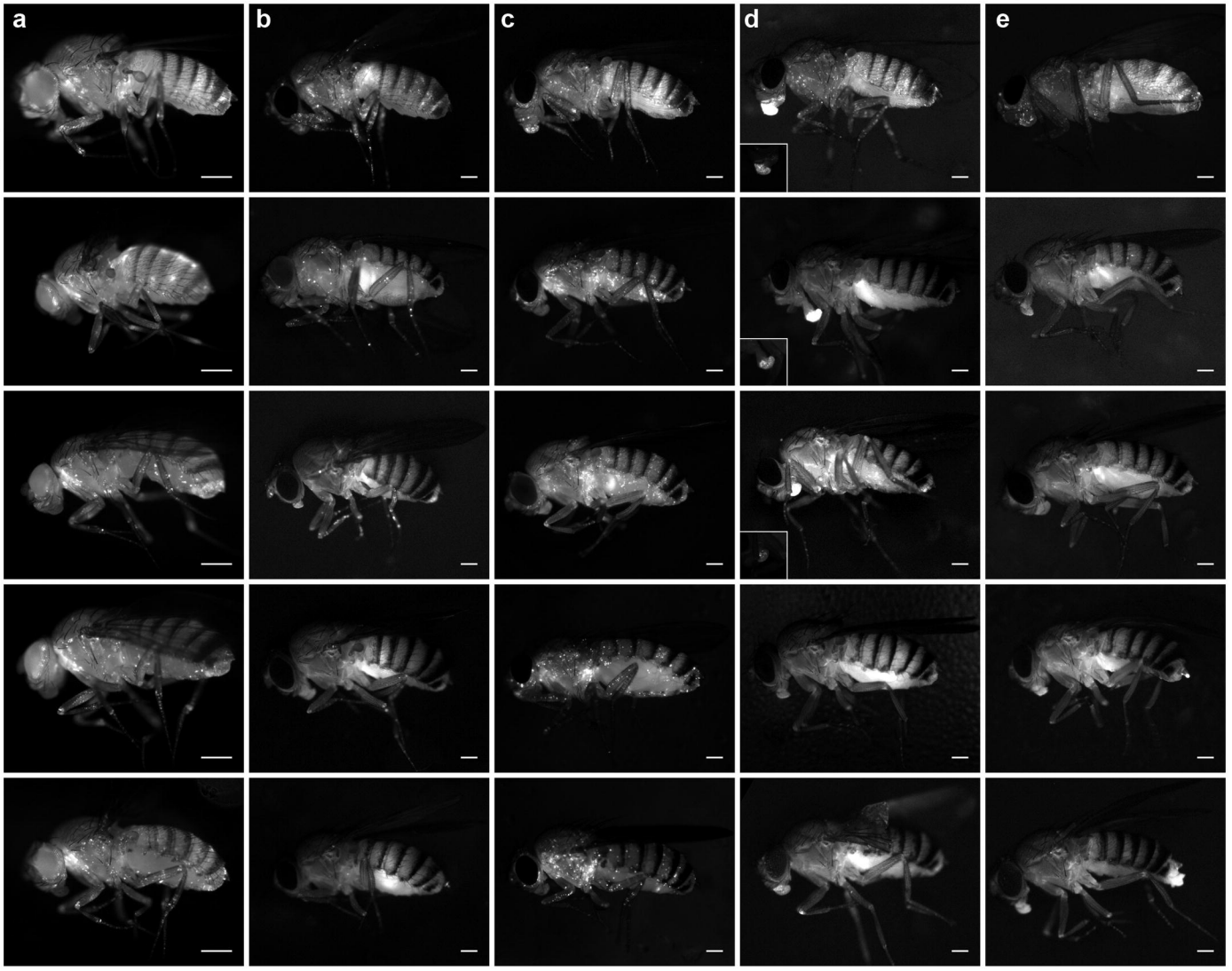
UAS-stinger
+ve con srp-3x-mCherry
srp-AD;VT17559-DBD
srp-AD;VT32897-DBD
srp-AD;VT57089-DBD
srp-AD;VT62766-DBD
a
b
c
d
e
day 1 post-eclosion
1 week
2 weeks
4 weeks
6 weeks

Figure 6

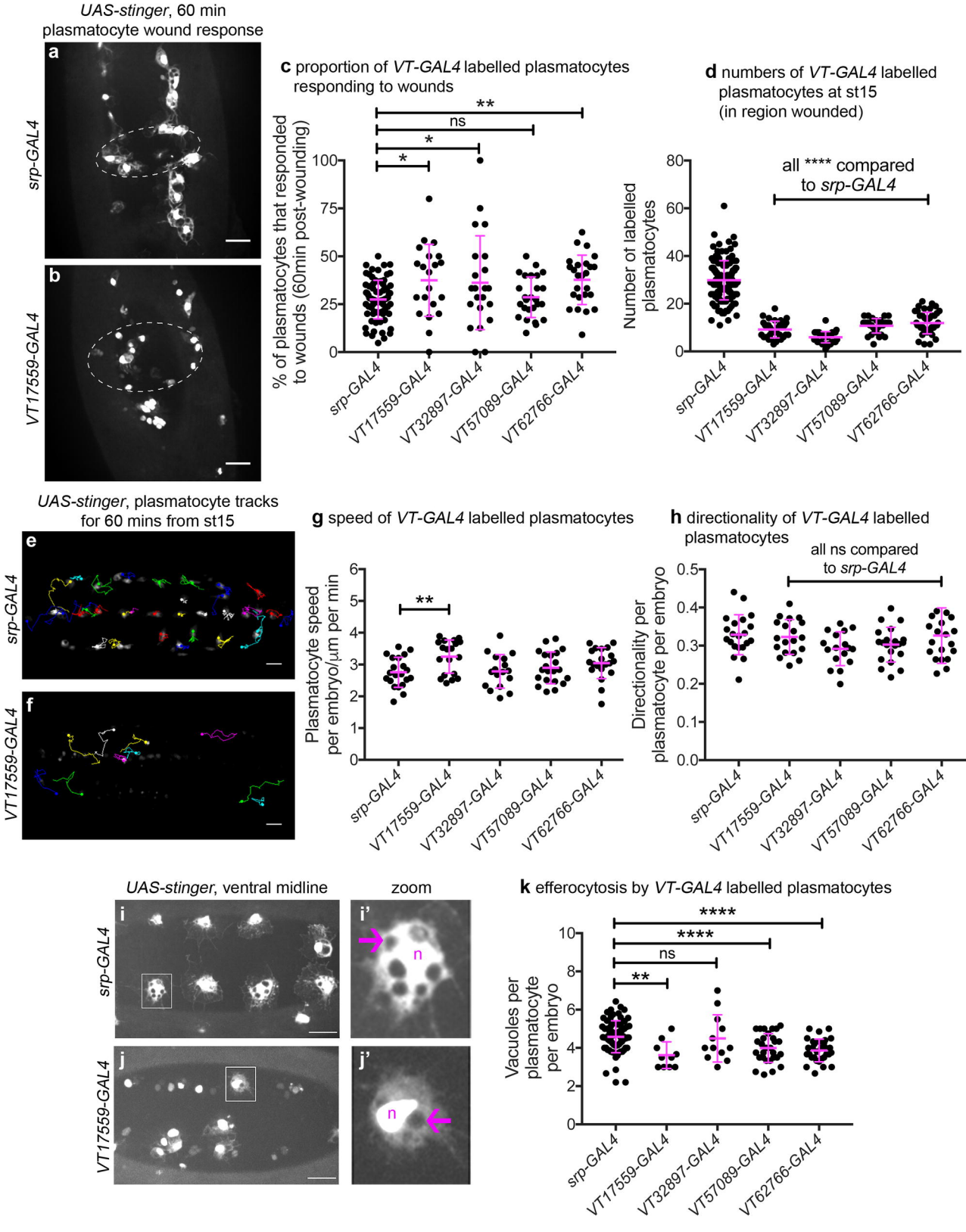
UAS-stinger, 60 min plasmatocyte wound response
a
b
srp-GAL4
VT17559-GAL4
c proportion of *VT-GAL4* labelled plasmatocytes responding to wounds
% of plasmatocytes that responded to wounds (60min post-wounding)
**
ns
*
*
d numbers of *VT-GAL4* labelled plasmatocytes at st15 (in region wounded)
Number of labelled plasmatocytes
all **** compared to *srp-GAL4*
srp-GAL4
VT17559-GAL4
VT32897-GAL4
VT57089-GAL4
VT62766-GAL4
UAS-stinger, plasmatocyte tracks for 60 mins from st15
e
f
g speed of *VT-GAL4* labelled plasmatocytes
Plasmatocyte speed per embryo/μm per min
**
h directionality of *VT-GAL4* labelled plasmatocytes
Directionality per plasmatocyte per embryo
all ns compared to *srp-GAL4*
UAS-stinger, ventral midline
zoom
i
i'
j
j'
n
k efferocytosis by *VT-GAL4* labelled plasmatocytes
Vacuoles per plasmatocyte per embryo
****
****
ns
**

Figure 7

a genomic location of *VT62766* enhancer region (X Chromosome)

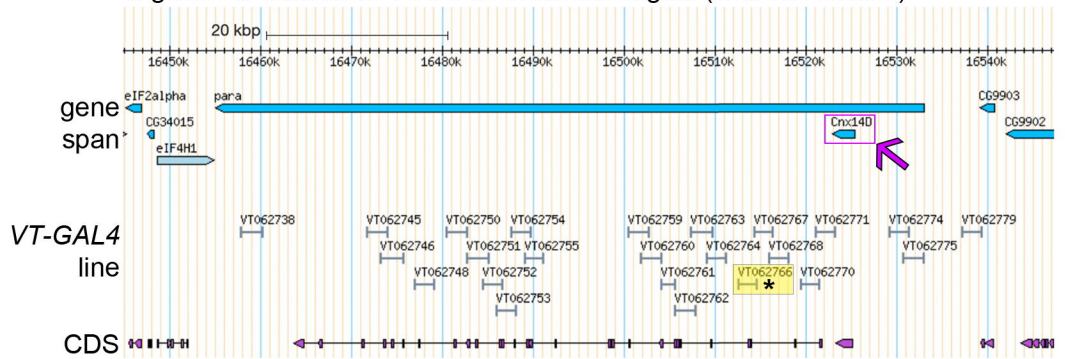

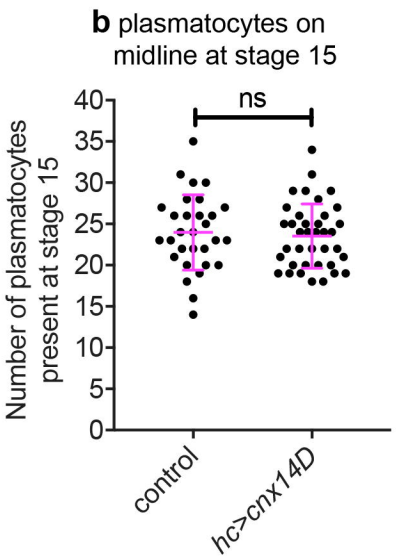

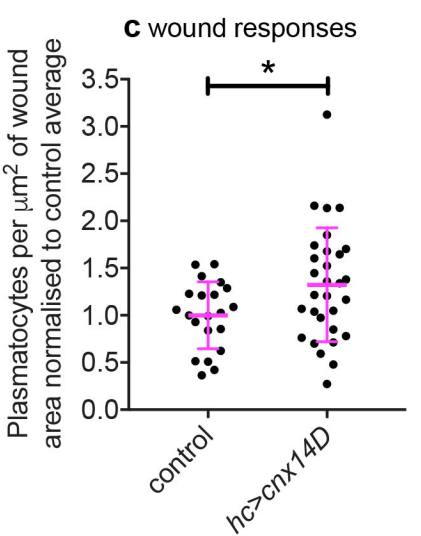

Figure 8

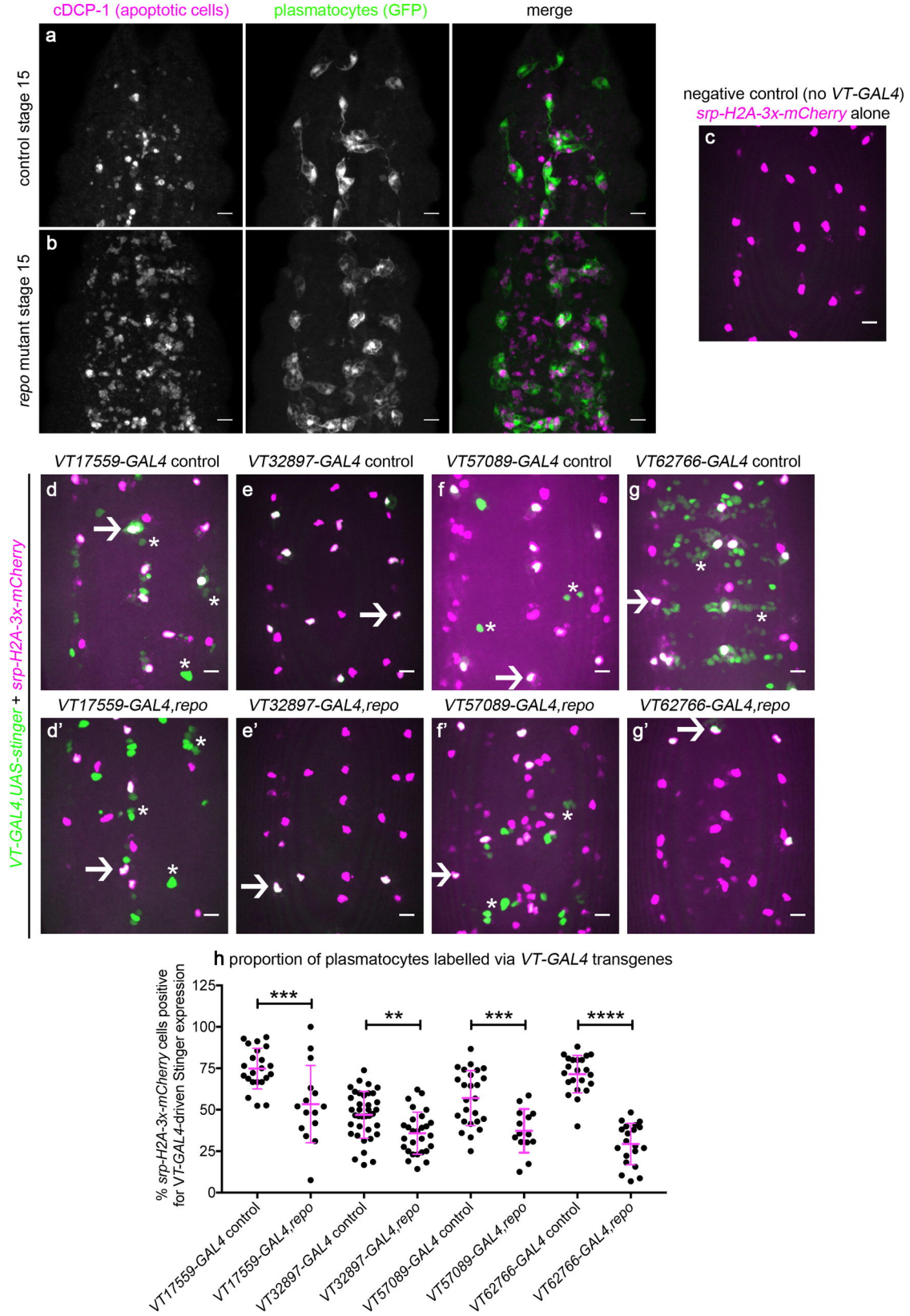
cDCP-1 (apoptotic cells)
plasmatocytes (GFP)
merge
a
control stage 15
b
repo mutant stage 15
negative control (no VT-GAL4)
srp-H2A-3x-mCherry alone
c
VT17559-GAL4 control
VT32897-GAL4 control
VT57089-GAL4 control
VT62766-GAL4 control
d
e
f
g
VT-GAL4,UAS-stinger + srp-H2A-3x-mCherry
VT17559-GAL4,repo
VT32897-GAL4,repo
VT57089-GAL4,repo
VT62766-GAL4,repo
d'
e'
f'
g'
h proportion of plasmatocytes labelled via VT-GAL4 transgenes
% srp-H2A-3x-mCherry cells positive for VT-GAL4-driven Stinger expression
125
100
75
50
25
0
***
**
***
****
VT17559-GAL4 control
VT17559-GAL4,repo
VT32897-GAL4 control
VT32897-GAL4,repo
VT57089-GAL4 control
VT57089-GAL4,repo
VT62766-GAL4 control
VT62766-GAL4,repo

Table 1. Summary of plasmatocyte subpopulation characteristics and their developmental regulation

	Subpopulation characteristics (compared to overall population):					Subpopulations in:				
Subpopulation	Wound responses	Migration speed	Efferocytosis	ROS levels	Phagocytosis of *E. coli*	Embryos	Larvae	Pupae	Newly hatched adults	Aged adults
VT17559	↑	↑	↓	no difference	no difference	distinct subpopulation	very few cells labelled	large numbers labelled by 18h APF	large numbers present	largely absent by 2 weeks
VT32897	↑	no difference	no difference	no difference	no difference	distinct subpopulation (fewest cells)	few cells labelled + nephrocytes & garland cells (?)	large numbers labelled by 72h APF	large numbers present	labelled cells persist
VT57089	no difference	no difference	↓	no difference	no difference	distinct subpopulation	almost no cells labelled + Bolwig Organ (?)	steady increase in numbers labelled	large numbers present	largely absent by 1 week
VT62766	↑	no difference	↓	no difference	no difference	distinct subpopulation	almost no cells labelled	large numbers labelled by 48h APF	large numbers present	largely absent by 1 week

Table 2. VT enhancer region location and neighbouring genes

VT enhancer	Genomic region*	Nearest genes	Distance of enhancer from gene
VT17559	chr2R 12069698–12070780	*Lis-1* *CG8441* *Ptp52F*	overlapping 2929bp upstream 3887bp downstream
VT32897	chr3L 18631149–18633281	*MYPT-75D* *bora* *not*	overlapping 13299bp downstream 15921bp downstream
VT57089	chrX 4961770–4962316	*ovo* *CG32767* *CR44833*	overlapping 3290bp upstream 3870bp downstream
VT62766	chrX 16406666–16408777	*para* *cnx14D* *CG9903*	overlapping 10404bp upstream 26520bp upstream

* D. melanogaster Apr. 2006 (BDGP R5/dm3) Assembly

Data taken from http://enhancers.starklab.org/